8 Study of the Subsurface of a Landslide by Geophysical Methods

S.R. Pant
Department of Geography, Tribhuvan University
Kiritipur, Kathmandu, Nepal

The geophysical methods commonly used in site investigations are equally applicable for the study of landslides. These methods can furnish subsurface information regarding types of material, depth to water table and bedrock, slip surfaces, and displaced and intact masses. In order to obtain this information, however, it is necessary to design the survey in an appropriate way, and to use the appropriate data acquisition and data processing techniques.

This paper provides an overview of the geophysical methods that are commonly used in the investigation of landslides. Seismic refraction and electrical resistivity methods have been widely applied; seismic reflection and ground-penetrating radar methods, though not used routinely at present, may be useful for the study of morphology and material-type distribution within the subsurfaces of landslides. The electrokinetic (filtration) potential method is also useful for studying the intensity and direction of groundwater movement.

Data acquisition and processing techniques for seismic refraction and electrical resistivity methods are described in detail. Usually geophysical data are collected under less than ideal circumstances, and processing and interpretation based on theoretically simplified earth models can yield erroneous results. New techniques described in this paper are more likely to accommodate actual subsurface geological conditions.

The paper includes a description of selected case studies acquired, processed, and interpreted by the author. A landslide in Sichuan, China provides a comparative study of conventional and generalised reciprocal method (GRM) processing of seismic refraction data. Studies of landslides and critical slopes along the Arniko Highway and at the Khimti I hydropower project in Nepal illustrate the use of 2-D electrical profiling (also called electrical resistivity tomography (ERT) or subsurface imaging (SSI)), a recent development in geophysics that has received wide application in environmental, groundwater, glaciology, and engineering investigations. The results obtained by these data processing techniques and seismic refraction and geoelectrical methods demonstrate their use in producing images of real subsurface geology.

Introduction

Geophysical methods of investigation involve the measurement of fields associated with changes in physical properties (density, magnetic susceptibility, electrical conductivity, elasticity, and radioactivity) in the near-surface and subsurface of the earth. Changes in physical properties, both in vertical and lateral directions, may indicate discontinuities, or anomalies (i.e., an inhomogeneous distribution) in subsurface materials. (The physical source of an anomaly is termed the geophysical target.) By processing the data observed on the surface, parameters related to the physical properties, depth, and size, of the subsurface layers and/or bodies that are creating the fields may be estimated. This process of estimating parameters of objects from observed fields is known as inverse solution. Data received from geophysical surveys can convey useful information about subsurface features such as geology, water table levels, buried cultural structures, and contaminant plumes, quickly and relatively inexpensively.

Geophysical methods have been widely applied in hydrocarbon, mineral, and groundwater exploration, glacier, permafrost, and landslide studies, engineering site investigations, the mapping of archaeological remains, and the location of buried pipes and cables. Hydrocarbon exploration remains by far the most common application of geophysical methods, but their use in environmental studies – for example, mapping variations in pore-fluid conductivity to indicate pollution plumes within groundwater – appears to be expanding significantly (Reynolds 1997). The same geophysical principles can be used in investigations ranging from a few metres to tens of kilometres in depth.

Applied geophysics provides a wide range of very useful and powerful tools when used correctly and in the right situations. Large areas can be surveyed quickly and in detail at relatively low cost. Moreover, geophysical methods are for the most part environmentally benign: there is no disturbance of subsurface materials. This is especially useful for the study of hazard areas.

Both the engineering and environmental aspects of landslides may be studied and monitored by geophysical methods. Site investigations usually entail the study of such engineering concerns as material types, depths to water table and bedrock, and locations of possible slip surfaces. By using time-series observations of different geophysical fields (such as geomagnetic, geoelectrical, electrokinetic (filtration) potential, and seismic velocity), the subsurface condition of a landslide can be assessed and the information can be used for risk analysis.

Methods of Investigation

Periodic saturation and dewatering of clayey and silty materials leads to changes in volume. This disturbs the structural relationships between materials in a slope and decreases the friction and cohesive forces that hold them together. Consequently the geophysical characteristics of a sliding area are likely to be different from those of a stable area (Novitskii 1974).

The study of landslides requires information on slopes, material types, and the thickness, physical properties, and water saturation of different layers. Geophysical methods can be used to detect different material types with different physical properties and/or for the differentiation of physical properties between sliding and intact masses within the same material type (Bogoslovsky et al. 1977).

Several of the available geophysical methods – based on seismic refraction, seismic reflection, electrical resistivity, filtration potential, and others – can be used to investigate landslides. Seismic refraction and electrical resistivity methods are widely used at all stages of landslide and other critical-slope investigations. These methods were already used in the late 1950s to study material types, slip surfaces, and water tables in the Alps and Caucasus (Klushin 1968) and their use has grown steadily since then, thanks to substantial improvements in the quality of equipment and data interpretation techniques. Since the late 1980s, the electrical resistivity method has evolved from 1-D to 2-D and even 3-D, while the interpretation of seismic refraction data has incorporated high-resolution processing. Mauritsch et al. (2000) have described a combined approach based on the interpretation of results from several different geophysical methods.

Seismic methods

In seismic methods, a signal is generated by vibrating to test the extent to which earth materials can be stretched or squeezed, somewhat like a sponge. Propagation of the vibration (seismic wave) causes the particles of a material to be stretched temporarily out of their position. The capacity of

a material to be temporarily deformed by seismic waves – its properties of elasticity – can be used to distinguish different types of materials. As these waves pass through subsurface media they are reflected and refracted back to the surface, where the returning signals are detected. The elapsed time between the source being triggered and the arrival of various waves is then analysed to determine the nature and dimensions of the subsurface layers.

The usual seismic sources are impulsive in nature. Seismic waves can be initiated by a dynamite blast, a shot from a shotgun using a blank cartridge, or the impact of a sledgehammer or dropped weight.

Physical and geological basis for seismic methods

When an external force (F) is applied across an area (A) of a surface of a body, forces inside the body are established in proportion to the external force. The ratio of the force to area (F/A) is known as stress. The stress applied to any surface can be resolved into two components, one at right angles to the surface (normal or dilatational stress) and the other parallel to the surface (shear stress). The stressed body undergoes strain, which is the amount of deformation expressed as the ratio of the change in length (or volume) to the original length (or volume). According to Hooke's Law, stress and strain are linearly dependent, and a body behaves elastically until the yield point is reached, i.e., the body reverts to its pre-stressed shape and size following relaxation of the stress. At stresses beyond the yield point, the body behaves in a plastic or ductile manner, and permanent damage results. If further stress is applied, the body is strained until it fractures.

Seismic waves, which consists of tiny packets of elastic strain energy, travel away from any seismic source at speeds determined by the elastic moduli (the constants that specify the relationship between stress and strain) and the densities of the media through which they pass. There are two main types of seismic waves: those that pass through the bulk of the medium are called body waves, while those that are confined to the interfaces between media with contrasting elastic properties, particularly the ground/air surface, are called surface waves.

There are two types of body waves that travel through elastic media: P-waves (also known as longitudinal, primary, push, or compressional waves) and S-waves (also known as transverse, secondary, or shear waves). The P- wave 'pushes and pulls' the rock it moves through in the same way that sound waves push and pull the air; in other words it radiates in the form of zones of compression separated by zones of dilation. The particle motion for P-waves is in the direction of the propagation (Figure 1a). In contrast S-waves move the rock up and down or side-to-side, i.e., the particle motion is at right angles to the direction of propagation (Figure 1b).

The velocity of the propagation of a seismic wave is given by the expression

$$V=(K/\rho)^{½} \qquad (1)$$

where V is the P- or S-wave velocity, K is the effective elastic parameter, and ρ is the density of the medium. K is a function of Lame's constants, λ and μ, which are related to how a material responds to normal and shearing stresses. The effective elastic parameter for P-waves is

$$K=\lambda+2\mu \qquad (2)$$

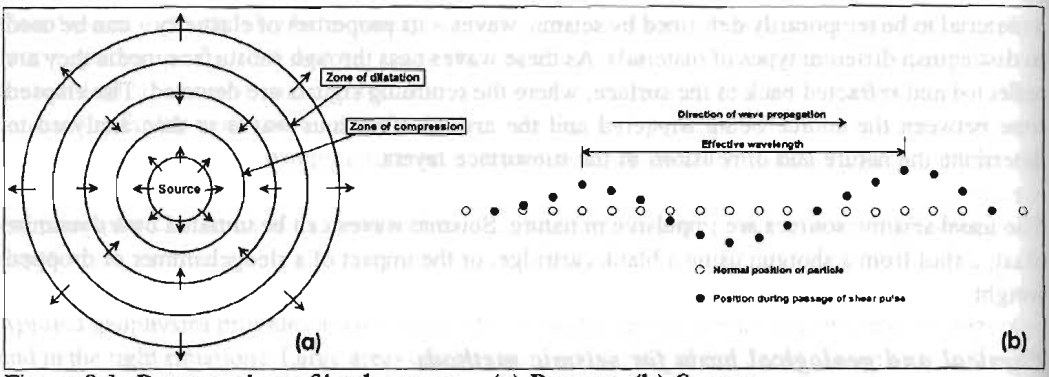

Figure 8.1: Propagation of body waves – (a) P-wave, (b) S-wave

and for S-waves

$$K = \mu \tag{3}$$

One of the most important parameters in seismic work is Poisson's ratio σ. If a cube of isotropic material (i.e., with the same properties in all directions) is stretched along one of its axes, the dimensions of the other two axes will decrease. Poisson's ratio is the ratio between the fractional lateral contraction and the fractional longitudinal extension of such a cube under tensile stress caused by a force from one direction.

Poisson's ratio can be expressed in terms of Lame's constants by

$$\sigma = \frac{\lambda}{2(\lambda + \mu)} \tag{4}$$

Or it can be expressed in terms of the P- and S-wave velocities, V_p and V_s, by

$$\left(\frac{V_p}{V_s}\right)^2 = \frac{(0.5 - \sigma)}{(1 - \sigma)} \tag{5}$$

For most consolidated rock material, V_p/V_s is between 1.5 and 2.0. By measuring the P- and S-wave velocities, Poisson's ratio can be calculated from equation (5). It can vary between the theoretical limits of 0 (a hard, rigid medium) and 0.5 (a fluid). Earth materials exhibit values for Poisson's ratio from about 0.05 for very hard rock to 0.45 for water-bearing unconsolidated materials (Sheriff and Geldart 1987). By measuring P- and S-wave velocities in a landslide, parameters and information needed for the stabilisation of the landslide can be deduced.

Equation (1) suggests that seismic velocity varies inversely with the square root of the density of the medium. However, P-wave velocity is higher for denser rock. An empirical relationship given in Gardner et al. (1974) shows the increase in P-wave velocity with density,

$$\rho = 0.31\, V^{1/4} \tag{6}$$

where ρ is density in g/cm³ and V is P-wave velocity in m/s. P-wave velocity also depends on the porosity and on the material filling the pores. The velocity generally increases as the porosity decreases. The relationship given by Wyllie et al. (1958) is

$$\frac{1}{V} = \frac{\varphi}{V_f} + \frac{1-\varphi}{V_m} \quad (7)$$

where V_f and V_m are acoustic velocities in the pore fluid and the rock matrix, and φ is fractional porosity.

The P-wave velocities for some materials commonly encountered in landslides are given in Table 8.1. These values are approximate and may overlap with the nearby ranges. It is essential to consider the geology and hydrogeology of a landslide area before interpreting the seismic data for material type. However, P-wave seismic velocity has a direct relationship with the strength and quality of a rock: the higher the velocity, the stronger the rock. This is true for materials below the water table (if the P-wave only is considered).

Table 8.1: **Approximate P-wave velocities for different materials commonly encountered in landslides or slopes**

Velocity (m/s)	Materials
200-400	very loose material above the water table
400-1500	unconsolidated clays and silts; unsaturated sands and gravels
1500-2000	saturated sands and gravel; compacted clays and silts; completely weathered rocks
2000-2500	partially consolidated sediments, probably water saturated; highly weathered and/or fractured metamorphic and igneous rocks; weathered and/or jointed sandstones and shales
2500-3700	partially weathered to fresh shales and sandstones; weathered and/or sheared metamorphic or igneous rocks or limestones
3700-4500	slightly weathered and/or fractured metamorphic or igneous rocks or limestones; some very hard or indurated sandstones and shales
4500-6000	unweathered metamorphic and igneous rocks; some limestones and dolomites

In addition to body waves, there are two types of **surface waves**, Rayleigh waves and Love waves (Figure 8.2). Rayleigh waves travel along the free surface of the earth in the same way that a wave rolls across a lake or an ocean, moving the ground up and down or side-to-side in the same direction that the wave is moving with amplitudes that decrease with depth. The particle motion is actually a retrograde ellipse in a vertical plane with respect to the direction of propagation. Love waves occur only where a medium with a low S-wave velocity overlies a layer with a higher S-wave velocity. Love waves move the ground from side-to-side, i.e., the particle motion is parallel to the surface, at right angles to the direction of wave propagation. Surface waves can be used to determine ground stiffness in situ. These waves somewhat mask the arrival of body waves; this masking effect can be filtered out in subsequent processing of seismic data. The velocity of surface waves is less than or equal to that of shear waves.

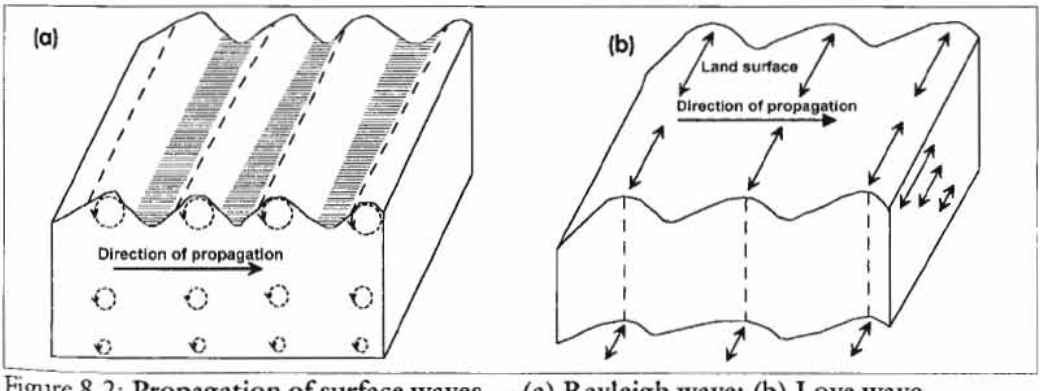

Figure 8.2: **Propagation of surface waves — (a) Rayleigh wave; (b) Love wave**

The amplitude of a seismic wave decreases as it travels away from the source – called **attenuation**. Attenuation results from the spherical spreading of the wave and from loss from absorption due to frictional dissipation of elastic energy into heat. Both mechanisms of attenuation for a homogeneous material are combined in the equation

$$I = I_0 \frac{r_0}{r} e^{-\alpha(r-r_0)} \qquad (8)$$

where I and I_0 are the amplitudes at distances r and r_0 from the source, and α is the absorption coefficient (Dobrin and Savit 1988). Experiments with different rock types show that higher-frequency energy has a greater absorption rate than does lower-frequency energy. This property of rocks causes a progressive lowering of the apparent frequency of seismic waves with increasing distance of travel through the earth.

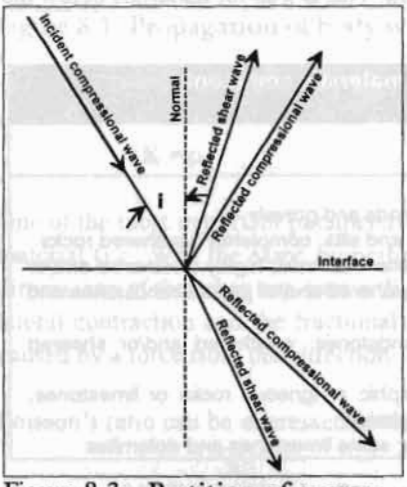

Figure 8.3: **Partition of energy of an incident compressional wave at an interface**

Whenever a wave impinges upon an interface across which there is a contrast in elastic properties, some of the wave's energy is reflected back off the interface – **reflection**, and the remainder passes through the boundary and is refracted on entering the second medium — **refraction** (Figure 8.3). The relative amplitudes of reflected and transmitted (refracted) seismic waves depend on the seismic velocities and densities of the two layers (Sheriff and Geldart 1987). The product of density (ρ) and velocity (V) for a given layer is its acoustic impedance. The reflection coefficient R gives the relative amplitudes of reflected waves. This can be expressed for a P-wave when the wave impinges at a right angle (normal) to the interface (Dobrin and Savit 1988) as

$$R = \frac{A_r}{A_i} = \frac{(\rho_2 V_{p2} - \rho_1 V_{p1})}{(\rho_2 V_{p2} + \rho_1 V_{p1})} \qquad (9)$$

When a P-wave impinges at an oblique angle to an interface it produces both reflected and refracted P- and S-waves. The angles made by the incident, reflected, and refracted waves with the perpendicular to the interface are called the angles of incidence, reflection, and refraction. The angles of incidence and reflection for P-waves are equal. However, the velocity of S-waves is smaller than for P-waves, which causes the angles of reflection and refraction for S-waves to be smaller than the angles of incidence and refraction for P-waves.

Seismic reflection method

Seismic reflection is the most commonly used method in hydrocarbon exploration. However, this method has not been applied as much as it could be in engineering and environmental investigations. Since around 1980 seismic reflection has been widely used for mapping Quaternary deposits, buried rock valleys, and shallow faults (Reynolds 1997). It can also be useful in the study of major landslides, since it has the capability of providing detailed subsurface images.

The essence of the seismic reflection technique is to measure the time taken for a seismic wave to travel from a source down to the interface and back to the surface, where it is detected by a receiver or detector. Such a receiver, called a geophone, converts ground motion into electrical energy. The output of a geophone is further filtered, amplified, and recorded on a seismograph. The record of each geophone is called a trace. A group of traces make a seismogram. The directions of wave propagation of the seismic waves can be shown schematically in the form of a 'raypath' diagram (Figure 8.4a).

The time a seismic wave takes to travel from source to detector, known as two-way travel time, can be calculated as follows:

$$(SO)^2 = 4h^2 + x^2$$

$$(Vt)^2 = 4h^2 + x^2$$

$$\frac{V^2t^2}{4h^2} - \frac{x^2}{4h^2} = 1 \qquad (10)$$

where S is the position of the source, O is the position of the reflector (reflecting surface), t is the two-way travel time, h is the depth to the reflector, V is the velocity of the seismic wave, and x is the distance from source to detector.

As the distance between the source and detector (x) is increased, the wave's two-way travel time (t) increases at twice the rate: thus the plot of t against x is a hyperbola (Figure 8.4b). Several hyperbolic forms of waves reflected from different interfaces can be observed on a seismogram.

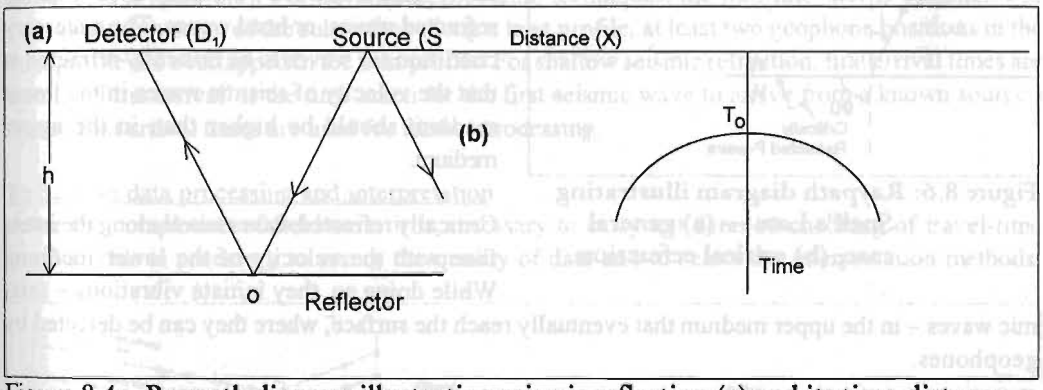

Figure 8.4: **Raypath diagram illustrating seismic reflection (a) and its time-distance graph (b)**

One of the principal reasons for the increased use of shallow seismic reflection is the improvement in equipment capabilities and the availability of microcomputers for processing. The equipment produced recently is portable and can be carried by one person. New equipment for shallow-depth studies can be used for both seismic reflection and refraction, and can record both P- and S-waves. The reflection method has been applied in groundwater investigations and in glaciology and palaeontology (Reynolds 1997; Geissler 1989).

Nowadays almost all reflection data are acquired and processed by the common midpoint (CMP) technique, which helps to enhance the signal/noise ratio. In this technique, a signal is emitted from

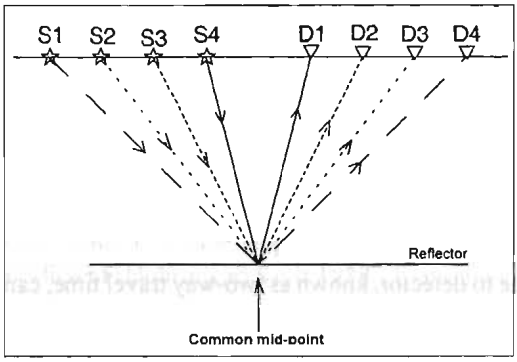

Figure 8.5: The principle of the common midpoint (CMP) technique

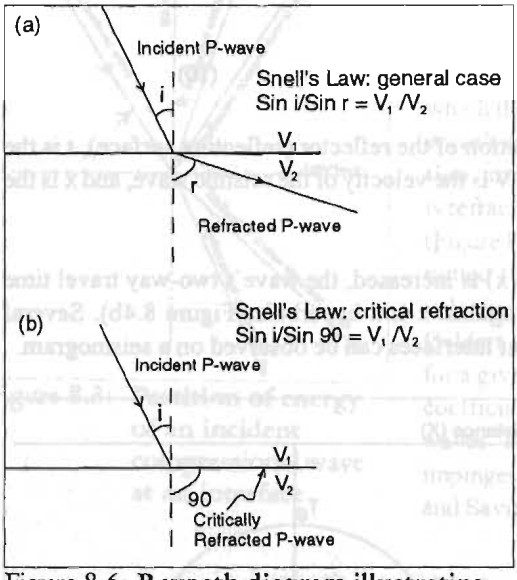

Figure 8.6: Raypath diagram illustrating Snell's Law — (a) general case, (b) critical refraction

multiple sources, and reflections arising from the same point on the interface – known as the common midpoint (CMP), common depth point (CDP), or common reflection point (CRP) – are detected by different geophones placed at the surface (Figure 8.5). The waves reflected from this point are summed after necessary corrections have been made to each trace signal; this summing tends to strengthen the coherent signals and reduce incoherent noise (for more details see Reynolds 1997; Robinson and Coruh 1988). Seismic reflection results are usually presented in the form of a time section. Depth sections are produced if needed and if the distribution of seismic velocities is known.

Seismic refraction method

When a seismic wave impinges on an interface, a portion of it is refracted – transmitted at a different angle – through the interface. According to Snell's law, which defines the relationship between a wave's incident and refracted angles, there is a certain critical angle of incidence that produces an angle of refraction of 90° (Figure 8.6). Such waves are called critically refracted waves, or head waves. The necessary condition for waves to be critically refracted is that the velocity of seismic waves in the lower medium should be higher than in the upper medium.

Critically refracted waves travel along the interface with the velocity of the lower medium. While doing so, they initiate vibrations – seismic waves – in the upper medium that eventually reach the surface, where they can be detected by geophones.

The time-distance relationship for an ideal two-layer case is given by the equation

$$t_x = \frac{x}{V_2} + \frac{2h_1 \cos i}{V_1} \qquad (11)$$

where t is time, x is distance, V_1 and V_2 are the velocities of seismic waves in the first and second (refractor) layer, and h is the depth of the refractor. Equation (11) is in the form of a straight line. The second term on the right hand side of the equation is the intercept of the refracted line with the time axis; this is called the intercept time.

Similarly the time-distance relationship for a multi-layered (n-layered) case can be calculated by the formula

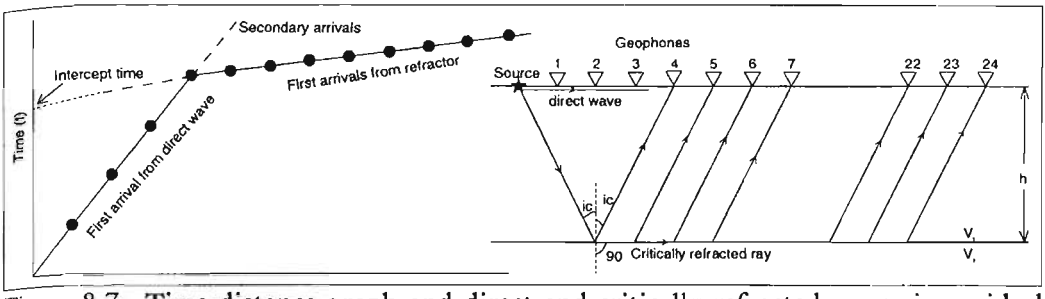

Figure 8.7: **Time-distance graph and direct and critically refracted waves in an ideal two-layer case**

$$t_x = \frac{x}{V_n} + \sum_{j-1}^{n-1} 2h_j \frac{\cos i_j}{V_j} \qquad (12)$$

Refraction data acquisition

In conventional methods of data interpretation, the subsurface is considered to be made up of horizontal or dipping planar interfaces. For the gross estimation of velocities and depths below each shot point (the gunshot or wave source), only two shots per spread are required: forward shot and reverse shot (Figure 8.8). However, this is not appropriate in a landslide investigation, as it tends to oversimplify the geological settings of the site.

For non-planar interfaces, a data acquisition procedure that is able to provide full coverage of the refractor is necessary. The processing and interpretation methods also make demands on the field operation. Three additional shots – off-end forward, off-end reverse, and mid-line – should be conducted (Figure 8.8). For advanced processing techniques, the mid-line shot is optional. For continuous coverage of the subsurface along a long profile, at least two geophone positions in the first profile are overlapped in the next profile. For shallow seismic refraction, first arrival times are noted. ('First arrival' is the time taken for the first seismic wave to arrive from a known source.) These first arrival times are used for further processing.

Refraction data processing and interpretation

After the completion of fieldwork, it is necessary to carry out detailed checking of travel-time graphs. This is necessary to assure the quality of data and to select the interpretation methods,

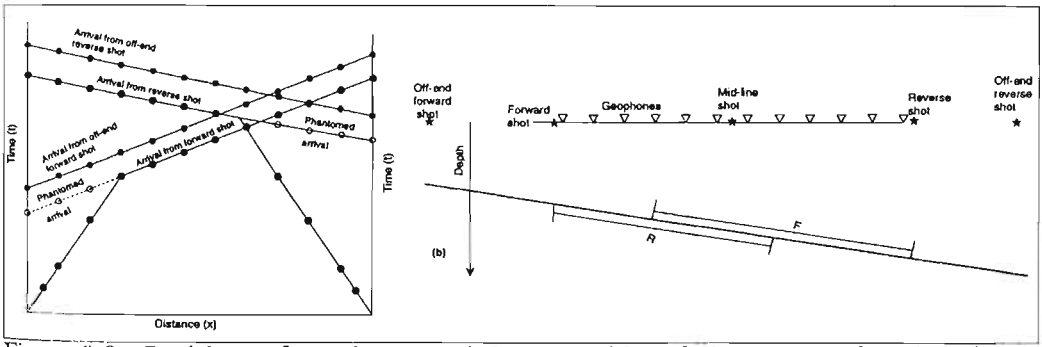

Figure 8.8: **Positions of geophones and shots to achieve full coverage of a subsurface (a), and time-distance graphs for a subsurface model (b). The segments of the refractor labelled 'R' and 'F' are those covered by the reverse and forward shots.**

and it may also help to optimise time and cost. During the selection of interpretation methods, the geological setting, morphology of the refractor, and probable thickness of the layer above the refractor (the overburden) of the landslide should all be considered. Among several methods of data processing and interpretation, only two are considered to be useful for landslide investigations. They are method t_0 and the generalised reciprocal method (GRM).

The first step in arranging time-distance graphs is **phantoming**. For the forward and reverse shots, there may be segments in the refractor where there is no overlap of the sort shown in Figure 8.8 (Lankston 1990). The travel times recorded for the off-end forward and off-end reverse shots are parallel to the travel times from the forward and reverse shots respectively. By shifting the travel-time curves of the off-end shots down in a parallel fashion, the first-break type arrival time for the section before the crossover distance can be reconstructed. Though not true arrival times, these so-called phantomed arrivals correspond to true arrival times. Determination of reciprocal time – the time taken for a wave to travel from the forward shot to the reverse shot or vice versa – is crucial for the interpretation of refraction data.

Method t_0 is a modification of the plus-minus method of interpretation originally proposed by Hagedoorn (1959) and helps determine the position of an undulating refractor. It is based on the following assumptions (Gurvich 1972):

- the refracted waves travel along the interface – that is, there is no effect of penetration in the refractor;
- the radius of curvature of the refractor's undulation is very high compared to the refractor's depth; and
- the refractor velocity does not have any sharp change.

After identifying the first breaks from the target refractor and performing the necessary phantoming calculations, the difference curve q(x) is calculated from the relationship

$$\theta(x) = t(x) - t'(x) + T \qquad (13)$$

where t(x) is the time reading at distance x in the forward phantomed curve; t'(x) is the time reading at distance x in the reverse phantomed curve; and T is the reciprocal time. The reciprocal times for the forward shot and reverse shot should be in good agreement. The target refractor velocity (V_b) is then calculated by taking the inverse of the slope of the curve θ(x)

$$V_b = 2\frac{\Delta x}{\Delta \theta} \qquad (14)$$

The change in the alignment of the points in the difference curve indicates the change in the velocity of the target refractor. The curve of the target refractor $t_0(x)$ and its depth h(x) are calculated for every x value using the following equations

$$t_0(x) = t(x) + t'(x) - T \qquad (15)$$

$$h(x) = K\, t_0(x) \qquad (16)$$

where $K = \dfrac{V_{av} V_b}{2\sqrt{V_b^2 - V_{av}^2}}$,

V_{av} is the average velocity of the overburden (above the target refractor) and V_b is the target refractor velocity.

The average velocity of the overburden is derived from the effective velocities, which are calculated by joining the lines from O to A and taking the inverse of the slope, where A is the start of the first break of the target refractor (Figure 8.9). The average velocity can be estimated from the effective velocities for forward and reverse profiles using

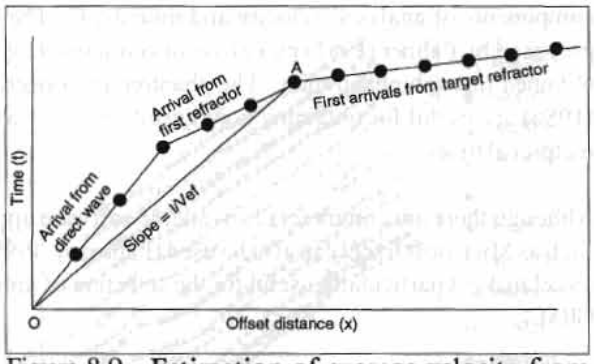

Figure 8.9: **Estimation of average velocity from effective velocity**

$$\frac{1}{V_{av}} = 0.5\left(\frac{1}{V_{ef1}} + \frac{1}{V_{ef2}}\right) \qquad (17)$$

where V_{ef1} and V_{ef2} are the effective velocities measured for the forward and reverse shots.

The estimation of average velocity from effective velocity works well for shallow depth investigations, and usually gives satisfactory results in cases where refracted waves are observed from all layers in the overburden. As the depth increases, however, the error in the average velocity determination also increases as a result of layering of the overburden, curvature of the refractor, and lithological change along the layer (Gurvich 1972). In a landslide, estimated average velocity will also be inaccurate if the layers are so thin that the arrival from these layers cannot be recorded.

An example of interpretation by method t_0 is presented in Figure 8.10. In this example, the t_0 (x) curve has a negative correlation with the refractor topography; θ(x) shows the possibility of several velocity changes along the target refractor. The depth calculation shows that the overburden is very thick. In general, the probability of layering within the overburden increases with its thickness. Furthermore, undulations in the refractor's topography may produce fictitious velocity changes in the target refractor. The reliability of the interpretation in such cases is discussed in more detail in the case studies.

The more sophisticated method called the **generalised reciprocal method (GRM)** should be used in an area where the overburden above the target refractor is relatively thick (probably more than 10m). When the overburden is thick, the assumptions used during an interpretation using the t_0 method may not reflect the real situation. Hidden layers and velocity inversions in the overburden are apt to distort the calculated depth. GRM is used for delineating an undulating refractor at any depth from in-line seismic refraction data consisting of forward and reverse travel times (Palmer 1981). GRM has two

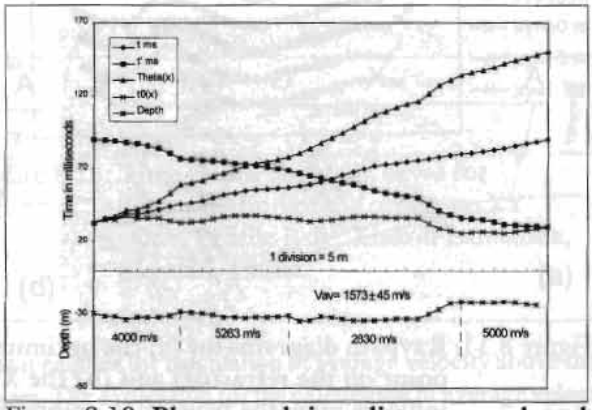

Figure 8.10: **Phantomed time-distance graph and its interpretation by method t_0, profile B-B', Xiakou Landslide, Sichuan, China (see also Figure 8.24)**

components of analysis: velocity and time-depth. The velocity and time-depth analysis function proposed by Palmer (1981) makes use of continuous forward and reverse direction profiles that are obtained through phantoming. The phantoming procedures described by Lankston and Lankston (1986) are useful for obtaining good results even in cases where it is difficult to find out reliable reciprocal times.

Although there are commercially available software applications for GRM, spreadsheet programs such as Microsoft Excel can also be used (Pant et al. 1999). The graphic presentation capabilities of Excel make it particularly useful for the selection of optimum velocity and time-depth functions in GRM.

Velocity analysis is the initial step in GRM processing. The velocity analysis function t_v is defined by the equation

$$t_V = \frac{t_{AY} - t_{Bx} + T}{2} \qquad (18)$$

where t_{AY} and t_{BX} are the arrival times for head waves from the forward and reverse shots that have emerged from the same point in the refractor and arrived at locations Y and X at the surface; and T is the reciprocal time (Palmer 1981). The value of the velocity analysis function is referred to G, which lies midway between X and Y (Figure 8.11a). With method t_0, XY is zero, which means the waves that emerge from the same point in the refractor arrive at the same point G on the surface (Figure 8.11b). In GRM, however, the velocity analysis is conducted using Palmer's minimum detail criterion (Palmer 1981) according to which the t_v curve that exhibits the least amount of irregularity is deemed to be the optimum one. The optimum XY is used in the later stages of GRM processing.

An example of velocity analysis is presented in Figure 8.12. To remove the overlapping of the curves, time has been added for each XY value. In Figure 8.12, the curves that exhibit the least amount of detail are for XY=45, 50, and 55m. The selection of any of these values is subjective. However, results will not be that much different. Each linear section in a velocity-analysis curve denotes one velocity zone in the target refractor. The inverse of the slope of each linear segment of the velocity curve is the velocity of the target refractor.

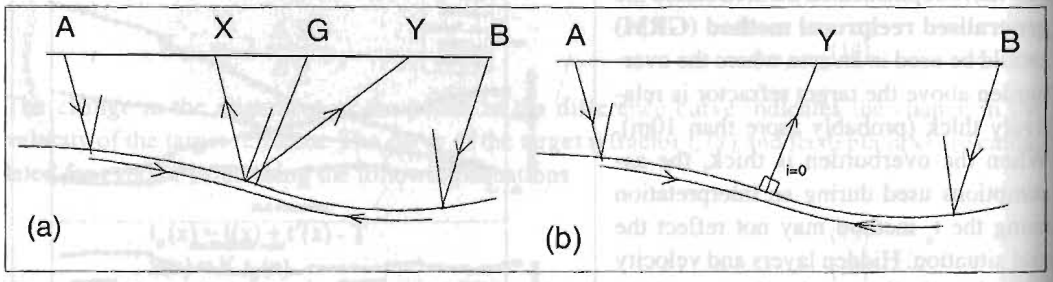

Figure 8.11: Raypath diagrams for (a) the optimum XY case (rays emerge from the same point on the refractor) and (b) the XY = 0m case. Lines with arrowheads indicate raypaths from shot points A and B to geophone points Y and X, respectively. The time to follow the path from A to B is the reciprocal time. X and Y represent one pair of geophone positions. Numerous pairs are used in GRM processing (Lankston 1990)

The process of restoring depth information from time information is called **migration**. It is important for the interpretation of both seismic refraction and reflection data. Time-to-depth migration is performed in two stages. The first is calculation and interpretation of the time-depth function t_G using the following formula

$$t_G = \frac{t_{AY} + t_{Bx} - \left(t_{Ab} + \frac{XY}{V_n}\right)}{2} \quad (19)$$

where V_n is the refractor velocity determined from the velocity analysis function (Palmer 1981).

Time-depth analysis shows more detail in the target refractor's topography than do other conventional methods, including method t_0. In time-depth analysis, the optimum curve – the one that best approximates the shape of the refractor – is the one with maximum displacement in bedrock topography. Note that both velocity and time-depth analysis should yield the same optimum XY values; in the case of a discrepancy, reanalysis can be conducted.

An example of time-depth analysis curves is presented in Figure 8.13. Again, the time values have been shifted relative to each other so that they do not overlap. In this example, the optimum XY value for the time-depth analysis function can be chosen as 45, 50, or 55m. Thus the optimum XY values as determined by velocity analysis and time-depth analysis are the same.

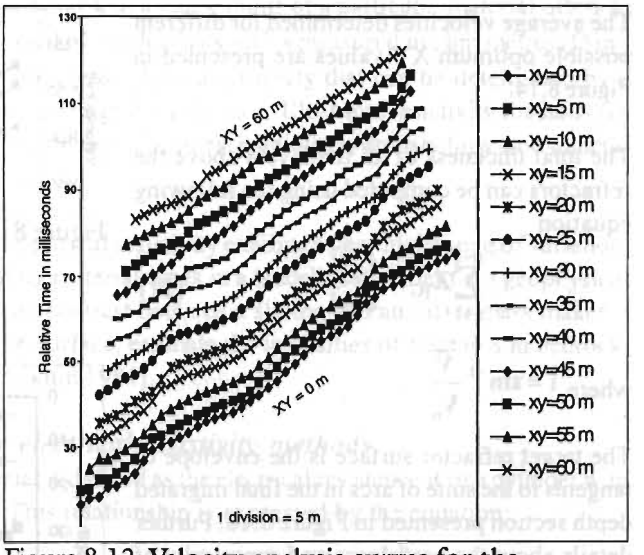

Figure 8.12: Velocity analysis curves for the determination of the optimum XY value, profile B-B', Xiakou Landslide, Sichuan, China

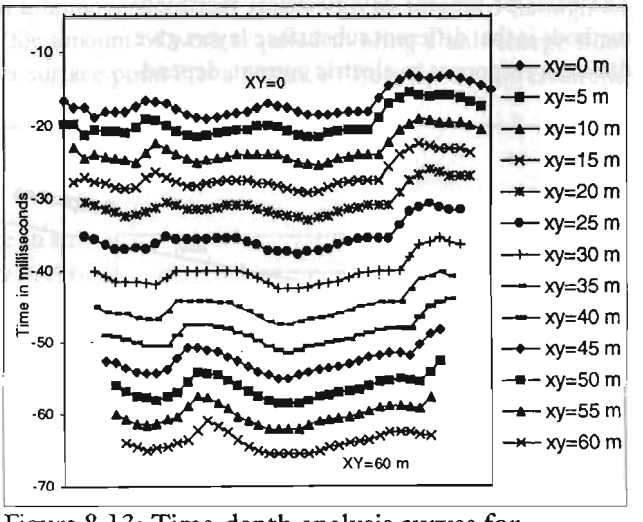

Figure 8.13: Time-depth analysis curves for determination of the optimum XY value, Profile B-B', Xiakou Landslide, Sichuan, China

One of the main advantages of GRM is that it enables the calculation of average velocity above the target refractor without defining all the layers. The expression for the calculation of average velocity is

$$\overline{V} = \left(\frac{V_n'^2 XY}{XY + 2t_G V_n'}\right)^{1/2} \quad (20)$$

The average velocities determined for different possible optimum XY values are presented in Figure 8.14.

The total thickness of all the layers above the refractors can be computed using the following equation

$$\sum_{j=1}^{n-1} Z_{jG} = \frac{t_G \overline{V}}{\cos \bar{i}} \qquad (21)$$

where $\bar{i} = \sin^{-1} \frac{\overline{V}}{V_n'}$

The target refractor surface is the envelope of tangents to the suite of arcs in the final migrated depth section presented in Figure 8.16. Further details about the usefulness and superiority of GRM is presented in the case studies.

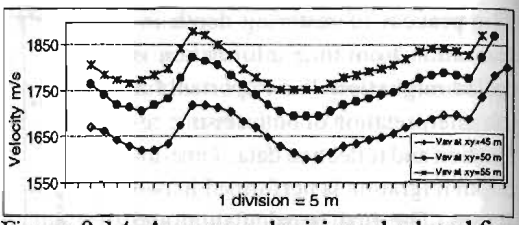

Figure 8.14: Average velocities calculated for different possible optimum XY values, profile B-B', Xiakou Landslide, Sichuan, China

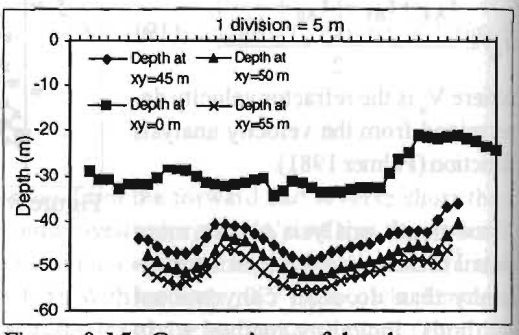

Figure 8.15: Comparison of depths calculated for different optimum XY values, profile B-B', Xiakou Landslide, Sichuan, China

Electrical Resistivity Methods

The basis of present day electrical resistivity methods is that different subsurface layers give different responses to electric current, depending mainly on their conductivity. The serious application of electrical resistivity methods dates back to before the First World War. At the beginning, two poles were used to send a current into the subsurface and conclusions were reached about the ground conductivity by measuring the amount of current; this provided information only about the conductivity of the surface near the grounding electrode. Later the four-pole system was developed in which two current electrodes were used to feed current to the subsurface and two potential electrodes measured the potential difference.

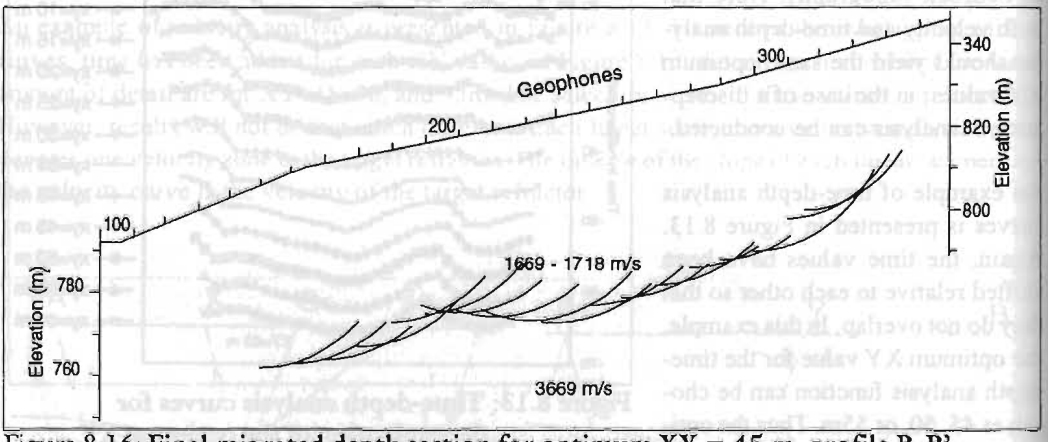

Figure 8.16: Final migrated depth section for optimum XY = 45 m, profile B-B', Xiakou Landslide, Sichuan, China

Electrical resistivity is the electrical resistance that a unit volume of a particular material offers to the flow of current at 0°C. It is the reciprocal of conductivity and is measured in ohm metres (Ω m). Electrical resistivity is a fundamental diagnostic physical property that can be determined by a wide variety of techniques, including electromagnetic induction. Electrical resistivity methods are widely used today in engineering and environmental studies, glaciology, archaeology, and mineral and groundwater exploration.

Compared to other physical properties, electrical resistivity exhibits a very high range of variation. This gives the possibility of differentiating material types in a landslide by other than geophysical methods (Novitskii 1974). The resistivity contrast between a sliding and an intact mass makes it possible to map the sliding mass and slip surface, estimate the intensities of fractures in bedrock, and forecast landslides (Brodovoe and Nikitin 1984).

Physical and geological basis for electrical resistivity methods

The electrical resistivity (ρ) of any material is defined as the electrical resistance R of a cylinder with a cross-section of area A and length l. This relationship is expressed by the equation:

$$\rho = R\frac{A}{l} \qquad (22)$$

Resistivity calculations are based on the following concepts.

A half-space is a model formed by only one plane surface; one example is a model with an air-earth interface. If a current I is injected into a homogeneous half space with resistivity ρ through an electrode at the surface, the potential (the amount of work required to bring a unit charge from infinity to the given point) V_p at another surface point P at a distance r from the source electrode will be

$$V_p = \frac{I\rho}{2\pi r} \qquad (23)$$

Let us consider a semi-infinite solid (like an air-earth interface) with uniform resistivity ρ. Assume that the current I is introduced into the ground through electrodes A and B and the potential difference is picked up between electrodes M and N (Figure 8. 17).

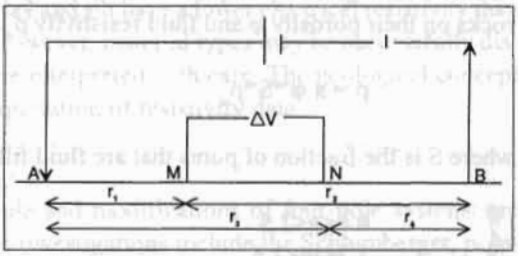

Figure 8.17: Arrangement of current electrodes (A and B) and potential electrodes (M and N)

The potential at M will be

$$V_M = \frac{I\rho}{2\pi}\left(\frac{1}{r_1} - \frac{1}{r_2}\right)$$

The potential at N will be

$$V_N = \frac{I\rho}{2\pi}\left(\frac{1}{r_3} - \frac{1}{r_4}\right)$$

The potential difference between M and N will be

$$\Delta V = V_M - V_N = \frac{I\rho}{2\pi}\left[\left(\frac{1}{r_1} - \frac{1}{r_2}\right) - \left(\frac{1}{r_3} - \frac{1}{r_4}\right)\right]$$

$$\rho = \frac{2\pi}{\frac{1}{r_1} - \frac{1}{r_2} - \frac{1}{r_3} + \frac{1}{r_4}} \cdot \frac{\Delta V}{I} \quad (24)$$

$$\rho = K\frac{\Delta V}{I} \quad (25)$$

where K is called the geometrical coefficient. If the resistivity is measured for inhomogeneous and anisotropic ground (i.e., without the same properties in all directions), the resistivity calculated by the above equation is called apparent resistivity and is denoted by ρ_a.

In electrical resistivity methods, DC or AC current of very low frequency (usually ≤10 Hz) is injected into the subsurface. Different geological formations, such as clay, silt, sand, gravel, boulders, and bedrock, will all respond differently. Bedrock, if it is weathered and fractured and saturated with water, will have lower electrical resistivity than fresh rock. In addition the different material types will usually have different degrees of porosity and permeability; for porous formations, electrical resistivity depends on the amount of water present and the salinity of the water.

Dry and unconsolidated, granular, and loose formations normally exhibit high resistivity values ranging from a few hundred to a few thousand Ohm metres. When saturated with water, the same formation will produce a much lower resistivity value due to the free conduction of electric current through water-filled pores. Thus an electrical resistivity of a saturated rock or sediment is a function of porosity, the electrical resistivity of the saturating fluid, the resistivity of the solid rock or sediment, the surface conduction of the rock or sediment, and the turtuosity of the fluid and electrical path. (Surface conduction is a form of ionic transport that takes place at solid-liquid interfaces by means of exchange mechanisms. Turtuosity is the length of the pore channel in which fluid migrates per unit length of the sample.)

Archie's Law gives an empirical relationship for the dependence of the resistivity of saturated rocks on their porosity φ and fluid resistivity ρ_w.

$$\rho = a\,\varphi^{-m}S^{-n}\rho_w \quad (26)$$

where S is the fraction of pores that are fluid filled; n=2; and a and m are constants with

$$0.6<a<2.5$$
$$1.3<m<2.5$$

For a saturated material equation (26) takes the form

$$\rho = a\,\varphi^{-m}\,\rho_w$$

The formation factor (F) is defined as the ratio of the electrical resistivity of the saturated formation to the electrical resistivity of the saturating water.

$$F = \rho/\rho_w = a\,\varphi^{-m}$$

In general for consolidated rocks

$$F = 1/\varphi^2 \quad (27)$$

For granular materials the relation is given by Humble's Formula

$$F = 0.81/\varphi^2 \quad (28)$$

The high formation factor for granular materials is an indication of their higher hydraulic conductivity (the measure of the relative ease of water flow under unequal pressure).

The resistivities of some rocks and other materials commonly encountered in landslides are given in Table 8.2. More extensive lists are given in Telford et al. (1976), Keller and Frischknecht (1966), and Reynolds (1997).

Table 8.2: Resistivities of granular materials and rocks commonly encountered in landslides

Material	Resistivity (Ωm)		
Marls	3 - 70	Granite	300 - 1,000,000
Clays	1-100	Schists (calcarious and mica)	20 – 10,000
Alluvium and sand	10 - 800	Schist (graphite)	10 - 100
Moraine	10 - 5000	Slates	10 - 100
Laterite	800 - 1500	Marble	600 – 40,000,000
Lateritic soil	120 - 750	Conglomerates	200 – 10,000
Quartz	300 – 1,000,000	Sandstones	1 – 740,000,000
Anthracite	0.001 – 200,000	Limestones	50 - 10,000,000
Lignite	9 - 200	Dolomite	350 - 5000

Table 8.2 shows that electrical resistivity varies considerably both within and between different types of material. Moreover, the resistivity ranges for different types of material overlap. In general rocks and formations made of fine materials like clay and silt have a lower electrical resistivity than do formations made of coarse-grained material. However, material types may be successfully distinguished using resistivity methods if the data are interpreted with care. The geological concept of landslides is important for the successful interpretation of resistivity data.

Electrode configurations

In modern electrical resistivity methods, four-pole and modifications of four-pole systems are used. Those that are or may be useful in landslide investigations include the Schlumberger, pole-pole, half-Schlumberger, Wenner (Wenner 1912), and dipole-dipole configurations (Figure 8.18). The Schlumberger and half-Schlumberger are the most commonly applied conventional configurations. The value of the apparent resistivity measured depends on the geometry of the electrode configuration. Different types of electrode configurations have certain advantages and disadvantages. It is up to the user to determine the suitability of a particular electrode configuration in a particular situation.

- **Schlumberger configuration.** In this configuration, the relationship between potential electrode distance (MN) and current electrode distance (AB) is MN £ (1/5) AB and the apparent resistivity is calculated as

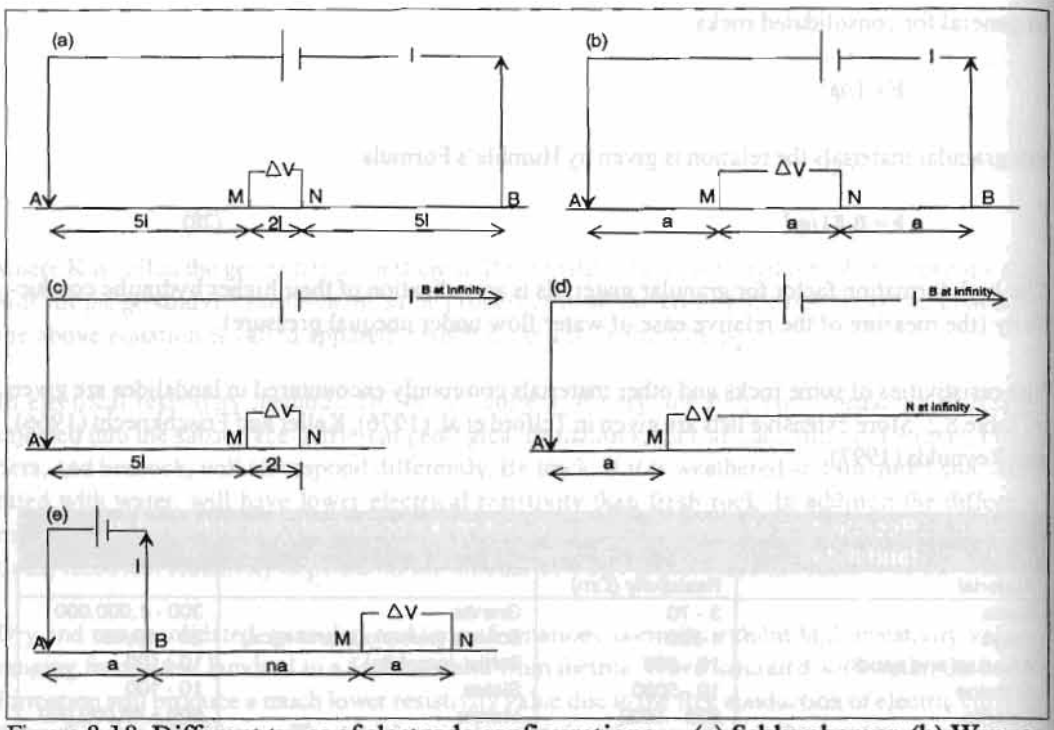

Figure 8.18: **Different types of electrode configurations — (a) Schlumberger, (b) Wenner, (c) half-Schlumberger, (d) pole-pole, and (e) dipole-dipole**

$$\rho_a = \pi \frac{AM\ AN}{MN} \frac{\Delta V}{I} \qquad (29)$$

- **Wenner configuration.** The inter-electrode distances are equal. The geometrical coefficient for this configuration is $2\pi a$, where a is the inter-electrode distance.
- **Half-Schlumberger configuration,** also called the three-point electrode configuration. One of the current electrodes, the remote electrode, is grounded at a remote position - at least 3.5 times the maximum distance between the centre and the current electrode), at right angles to the expanding profile. The geometrical coefficient is double that of the normal Schlumberger configuration.
- **Pole-pole configuration,** sometimes called the half-Wenner array. One current and one potential electrode are kept at the remote position. The potential difference measured between M, the measuring electrode, and N, the remote electrode, will be equivalent to the potential created by current electrode A. The geometrical coefficient is equal to $2\pi a$, where a is the distance between electrodes A and M.
- **Dipole-dipole configuration.** Two current electrodes, a positive electrode A and a negative electrode B, and two potential electrodes M and N, form dipoles if they are separated by a very large distance; the current dipole AB must be separated from the measuring dipole MN by a distance more than five times the dipole length (A to B or M to N, they are the same). The geometrical factor for the dipole-dipole method is $n(n+1)(n+2)\pi a$, where a is the dipole length and n is any integer.

A wide range of equipment is available to suit various purposes. Some setups are for shallow-depth investigations, others are for deep investigations. Because the grounding conditions in a landslide may not be favourable, the receiver of the equipment should have very high input

impedance (at least 10 MΩ). The basic requirement on a transmitter is that it can provide a constant-current source while this current is introduced into the ground. The use of very low AC current will help to minimise the polarisation effect (layering of electrical charge at the contact between an electrode and the ground). A microprocessor-controlled resistivity meter with a multi-electrode switching system is helpful for the detailed investigation of landslides in a short time.

In general the term 'depth of investigation' refers to the depth below which surface devices are insensitive to the value of the physical properties of the earth (Oldenburg and Li 1999). This depth depends on the distance between the current and potential electrodes and/or on the total length of the array (Edwards 1977). It also depends on the geology. By increasing the distance between the current and potential electrodes, information from a greater depth can be obtained. This can be achieved in different ways: by increasing the distance between the current electrodes and keeping the distance between the potential electrodes fixed, or by increasing the distance between the current and the potential electrodes.

Measurement procedures

There are three main procedures used in resistivity measurement: electrical profiling, vertical electrical sounding, and 2-D profiling (also called electrical resistivity tomography (ERT) or subsurface imaging (SSI)). Any of the electrode configurations can be used for electrical profiling and sounding measurements; pole-pole and Wenner configurations are usually used for 2-D profiling.

In **electrical profiling (EP)** profiling, inter-electrode distances are kept fixed, and the array of the electrodes is moved laterally along a profile, the apparent resistivity being plotted at midpoints. This is called continuous profiling or simple profiling. In profiling, the search depth remains the same throughout the profile. Profiling is used to find out lateral variations in resistivity. This method is useful for mapping loose, sliding, and intact masses in the slope, fracture zones in rocks, or steeply dipping contacts between different types of earth materials.

Vertical electrical sounding (VES) is conducted to find out resistivity variations with depth. This is done by increasing the distance between the outer current electrodes or by increasing the relative distance between the current and potential electrodes. The centre of the measurement is kept fixed. The curve is plotted on bi-logarithmic paper with electrode spacing versus apparent resistivity (Figure 8.19). This curve, known as a sounding curve, implies variations in electrical resistivity with depth.

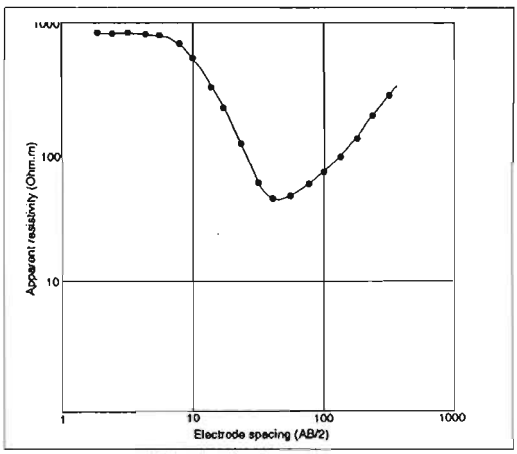

Figure 8.19: **Vertical electrical sounding curve, showing apparent resistivity as a function of electrode spacing (AB/2)**

The method of **2-D electrical profiling** is used to measure both vertical and lateral change in electrical resistivity. This can be considered as a combination of profiling and sounding. Increasing the distance between the current and potential electrodes produces the effect of sounding while shifting the current electrode along the measurement line produces the effect of conventional profiling (Figure 8.20). This method is useful for preparing electrical resistivity

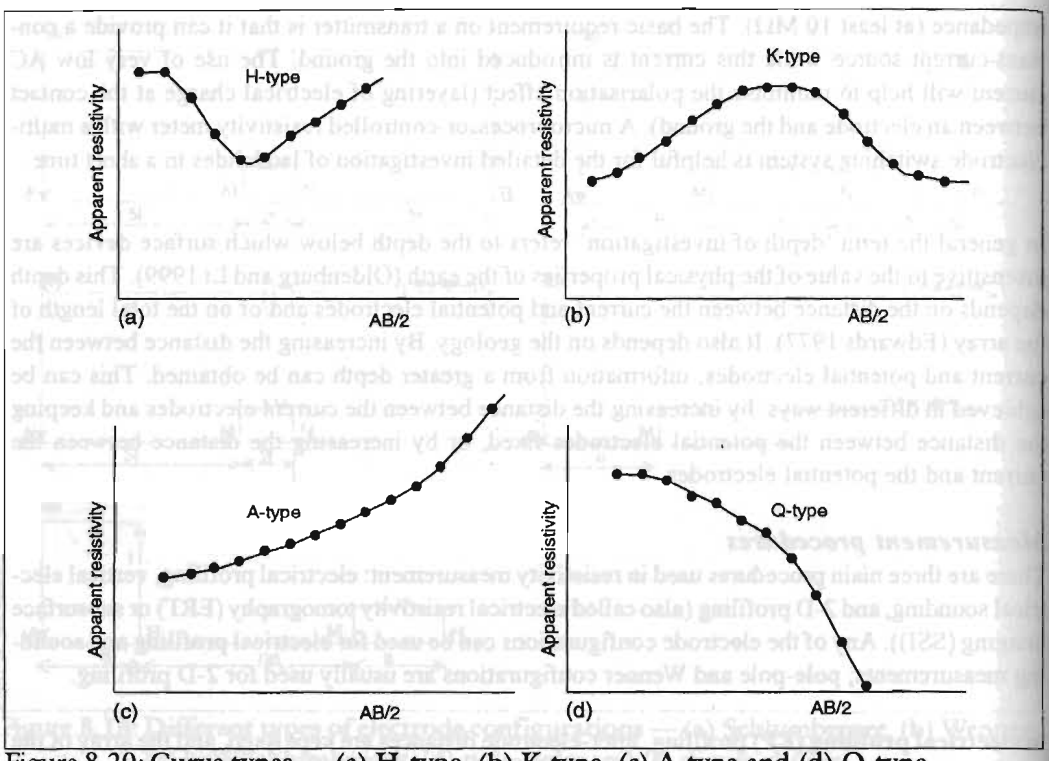

Figure 8.20: **Curve types — (a) H-type, (b) K-type, (c) A-type and (d) Q-type.**

tomograms (showing the variation in electrical resistivity across a 2-D section) of the subsurface of a landslide.

Interpretation of Data

The first stage in the interpretation of electrical resistivity data is **qualitative interpretation**.

Conventional electrical profiling data undergo only qualitative interpretation and the end products are apparent resistivity maps and profiles.

The subsurface under investigation may include a number of layers of a geological formation. Each layer of the formation will show certain values of electrical resistivity. VES curves are separated during qualitative interpretation according to curve types. Separating the curves by type and analysing them helps in the formation of a geoelectrical and geological concept of the study area; VES curves roughly show the geoelectrical characteristics of a site. Depending on the relative distribution of resistivity along a depth section, there may be different types of curves. For a three-layered section there are four different types of curves: H (bowl) type, K (bell) type, A (ascending) type, and Q (descending) type (Figure 8.21).

H-type	$\rho_1 > \rho_2 < \rho_3$
K-type	$\rho_1 < \rho_2 > \rho_3$
A-type	$\rho_1 < \rho_2 < \rho_3$
Q-type	$\rho_1 > \rho_2 > \rho_3$

where ρ_1, ρ_2, ρ_3 are the resistivities of the first, second, and third layers.

A combination of these types of curves can be obtained for sections with more than three layers.

During qualitative interpretation, VES data are usually presented as maps of curve types and apparent resistivity maps at different electrode spacings and sections. Maps at different electrode spacings are useful for the analysis of resistivity distributions at different depth levels. This information can be further used to estimate material type distributions.

Quantitative interpretation is based on mathematical analysis. Quantitative analysis is highly developed for VES data for depth probing. Interpretation of VES data is carried out by matching field curves against curves theoretically calculated by computer. Suitable parameters of the layers (true resistivity and thickness) that fit with geological concepts are chosen. The matching is made based on the assumption that the layers are horizontal. In the case of landslides, layers are assumed to be parallel to the surface of the slide. The final results are presented as geoelectric sections.

Recent developments in finite element processing techniques applied in electrical resistivity methods also make it possible to invert 2-D profiling data. Commercial 2-D resistivity imaging inversion packages are available from a number of sources. One such is RES2DINV. This program automatically determines a two-dimensional resistivity model for the subsurface using the data obtained from electrical imaging surveys. The 2-D model used by the inversion program consists of a number of rectangular blocks. The distribution of the block sizes is automatically generated by the program so that the number of blocks do not exceed the number of data points. The depth of the bottom row of blocks is set to be approximately equal to the equivalent depth of investigation of the data points with the largest electrode spacing (Edwards 1977). A finite-difference forward modelling subroutine is used to calculate the apparent resistivity values, and a non-linear least-squares optimisation technique is used for the inversion routine. The optimisation method basically tries to reduce the difference between calculated and measured apparent resistivity values by adjusting the resistivity of the model blocks. The software has different options that help to modify processing parameters to suit the nature of the data and the geological problems to be solved. The end product of such processing is an image of the true resistivity distribution of the subsurface. A subsurface that consists of bodies or layers can be produced by finite-element forward modelling. In this modelling, the resistivity response for a 2-D model is calculated and displayed as a pseudo-section for comparison with the original field data. This approach is useful for generating realistic subsurface geometries. The end products of the processing are called electrical resistivity tomograms.

Elektrokinetic (Filtration) Potential Method

The electrokinetic (filtration) potential method is a passive method: there is no need to create an artificial source as in the seismic and resistivity methods. The method measures the naturally occurring electrokinetic potential (also called zeta potential or filtration potential, the electric potential that exists across the interface of all solids and liquids). Electrokinetic potentials are related to the movement of groundwater in porous rocks. Favourable conditions for the formation of strong electrokinetic potentials are: a large pressure gradient on the filtering horizon, high resistivity (low mineralisation) of water, a shallow filtering horizon, high resistivity of the overburden overlying the filtering layer, and a narrow pore structure with high permeability (Semenov 1974). These conditions are fully satisfied in a landslide and other critical slopes. Although there are no publications related to the application of this method to landslides, there are reports of its successful use to detect leakage from a water reservoir (Bogoslovsky and Ogilvy 1970), leakage of contaminant plumes from a waste disposal site, and groundwater contamination (Corwin 1986; Schiavone

and Quarto 1984; Hughes et al. 1986). The method's application in other fields related to groundwater movements suggests that it could also be used to investigate shallow landslides.

Since electrokinetic potential measurement does not require an external source, only two electrodes are needed (to receive the signal). The receiving electrodes consist of a porous pot made of ceramic or wood that leaks a concentrated salt solution, usually copper sulphate, into the ground through which contact with the ground is maintained; the metal electrode is immersed in the solution. For the acquisition of data in a landslide, one of the potential electrodes is kept fixed outside the landslide and the other is moved to measure along a profile. The end products are presented as maps or profiles. The groundwater recharge area will be indicated as negative and the discharge area as positive potential areas. The area with predominant movement of groundwater will be indicated by relatively high-intensity potential areas.

Other methods

There are other methods that can be applied to the investigation of landslides, including the ground conductivity, electromagnetic, and ground penetrating radar (GPR) methods (Parasnis 1997; Reynolds 1997). All these methods may be useful for shallow depth investigations, usually ranging from a few metres to a few tens of metres.

Applications and Case Studies

The following case studies were carried out in landslides along the Arniko Highway and near the desilting basin of a hydropower project in Nepal, and near Yaan in Sichuan, southwest-central China. The location maps for these sites are presented in Figures 21 and 22.

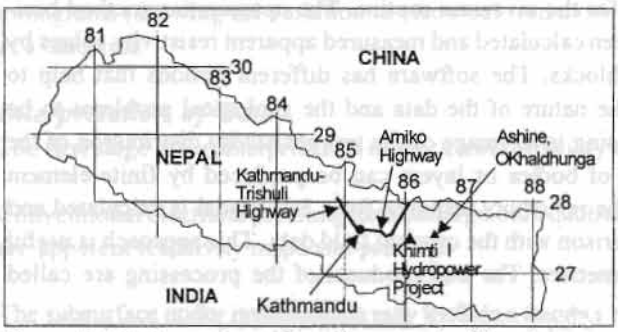

Figure 8.21: Location of study areas in Nepal

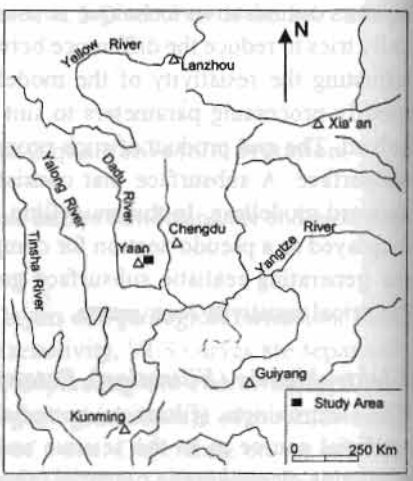

Figure 8.22: Location of study areas in south-west central China

Investigation of a landslide using Seismic Refraction and VES: Xiakou Landslide, Sichuan, China

Yaan, a small city in Sichuan, has been inundated by floods several times in the past, mainly due to the blocking of the Longxi River by a landslide. This landslide, known as the Xiakou Landslide, was identified as one of the study sites of the Mountain Risk Engineering, China Project (Figure 8.22). The slide is 9 km upstream of Yaan City.

Two methods were proposed for the investigation: seismic refraction and vertical electrical sounding (VES). The objectives of VES and seismic refraction were to decipher the overburden and

discover the depth to bedrock. During the interpretation and processing of field data, findings of both seismic refraction and VES were compared. The fieldwork was conducted during November 1995.

Previously the area had been studied by drilling a single borehole. The borehole showed a multi-layer sequence of gravel and boulders, and boulders mixed with clay. The bedrock consists of series of sandstone, claystone, and silty-claystone. As part of the geophysical investigation, the subsurface of the landslide was explored by five seismic profiles and 28 VESs. Due to the constraints in the available number of channels, the geophones were spaced at 10m intervals. With this spacing, it was only possible to obtain average information for the overburden. Most of the VESs were conducted using the Schlumberger configuration, and a few using the half-Schlumberger. The electrodes were expanded along the slope. The locations of the VES and seismic profiles are shown in Figure 8.23.

The VES curves were interpreted both qualitatively and quantitatively. They indicated that the water table was at a shallow depth (1-3m), and that a very low resistivity layer overlay the bedrock everywhere. One of the representative sounding curves is shown in Figure 8.24 together with the qualitative interpretation. The apparent resistivity map at electrode spacings (AB/2) of 8m is shown in in Figure 8.25. The idea behind the selection of this particular electrode spacing for mapping was to acquire information about the very shallow sliding layer. At very short electrode spacings (<5m), measurements may be highly affected by surface inhomogeneities. The apparent resistivity values can be roughly correlated with the material-type distribution in the near-subsurface. From the map, a coarse-grain-dominated material would be expected at a shallow depth in the north-east part of the area. The proportion of clay increases toward the south, south-east, and south-west parts of the area. The area dominated by low resistivity is more prone to mudslide than the others.

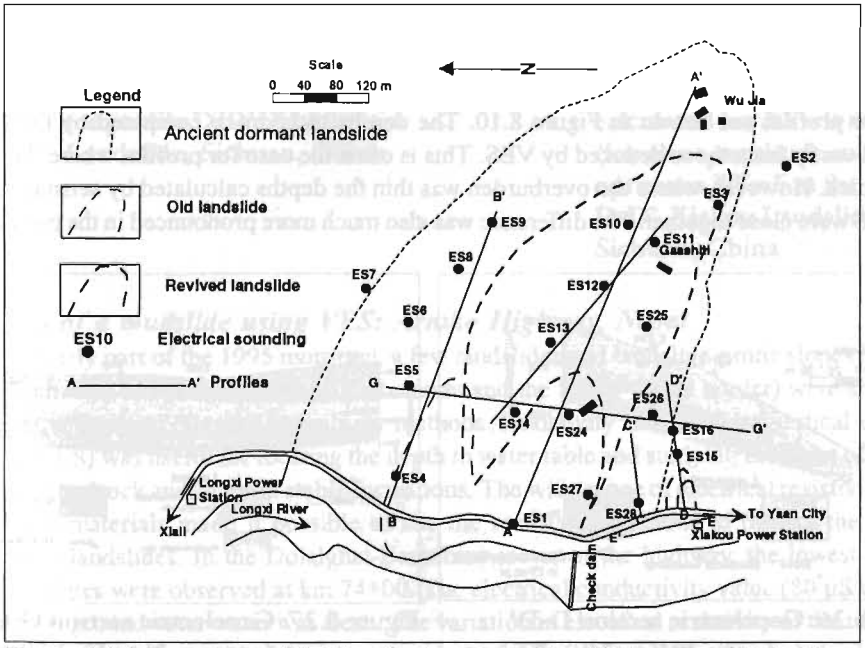

Figure 8.23: **Locations of VES and seismic profiles, Xiakou Landslide, Yaan, Sichuan, China.**

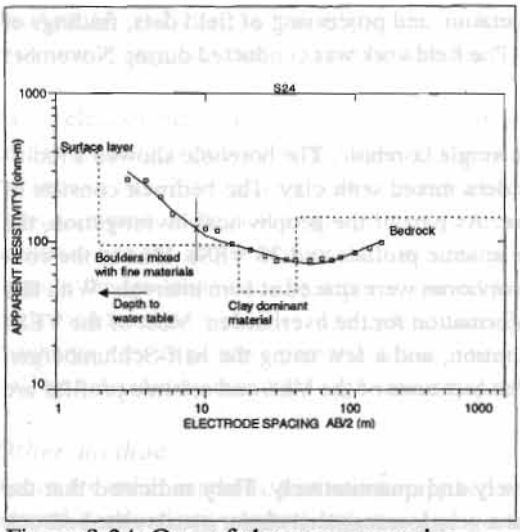

Figure 8.24: **One of the representative sounding curves and its curve matching results, Xiakou Landslide, Sichuan, China**

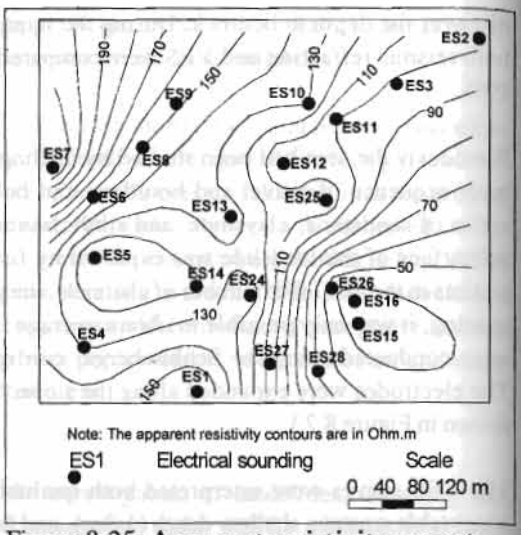

Figure 8.25: **Apparent resistivity map at electrode spacing (AB/2) of 8 m, Xiakou Landslide, Sichuan, China**

The results of the quantitative interpretation of the VES curves are presented as geoelectric sections D-D' and G-G' in Figures 8.26 and 8.27. Figure 8.27 shows a very thick overburden. The northern part of this profile reveals four electric layers, reducing to three in the south. The first layer is a very loose surface layer above the water table; the second is a cumulative effect from an accumulation of different layers of clay and boulders or clay and boulders mixed together; and the third is a clay-dominant material. The fourth electric layer effect is from bedrock. Geoelectric section D-D' (Figure 8.26) indicates only two layered media: the bedrock is overlain by a clay-dominant layer.

Seismic refraction profiles were interpreted using the t_0 method. The results for one of the representative profiles are shown in Figure 8.10. The depths to bedrock computed by the t_0 method differed vastly from those deduced by VES. This is often the case for profiles where the overburden is thick. However, where the overburden was thin the depths calculated by seismic refraction and VES were close together. The difference was also much more pronounced in the profiles where

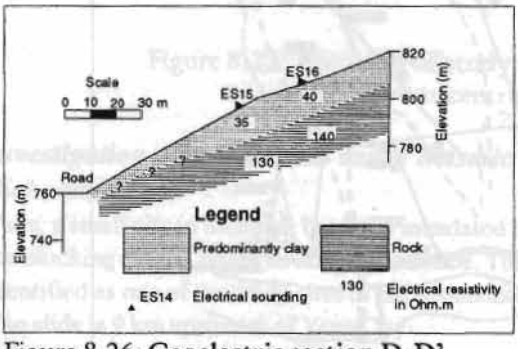

Figure 8.26: **Geoelectric section D-D' (approx. SW to NE), Xiakou Landslide, Sichuan, China**

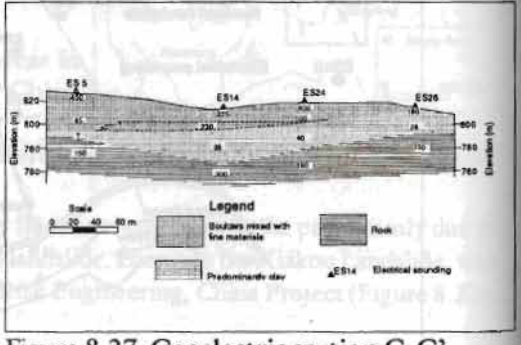

Figure 8.27: **Geoelectric section G-G' (approx. N to S), Xiakou Landslide, Sichuan, China**

more clay was expected. The velocity of the refractor deduced from the t_0 method is highly affected by bedrock topography. Due to the bedrock topography, several fictitious velocity changes were identified that were not compatible with the actual bedrock geology in the landslide (see Figure 8.10 for details).

To overcome this problem, all seismic profiles were processed using the generalised reciprocal method (GRM). Since there was no micro-seismic survey, it was not possible to make a detailed study of the overburden. Hence the objectives of the GRM processing were to determine depth to bedrock (target refractor) and to estimate the true refractor velocity. An average velocity of the overburden (above the target refractor) was calculated for optimum XY values. The final migrated sections of representative profiles B-B' and D-D' are presented in Figures 16, and 28 respectively; in these figures, the interface between the refractor and the overburden is tangent to the arcs. The results produced by GRM and the t_0 method were similar for profile D-D' but differed considerably for profile B-B'. The results of the GRM processing show again that the conventional method of interpretation can only be justified for shallow-depth investigations (less than 10-15 m; see Figure 8.29). When the results obtained by the t_0 method (Figure 8.10) and GRM (Figure 8.16) for profile B-B' are taken together, they indicate that the velocity changes along the bedrock indicated by the t_0 method result from the bedrock topography.

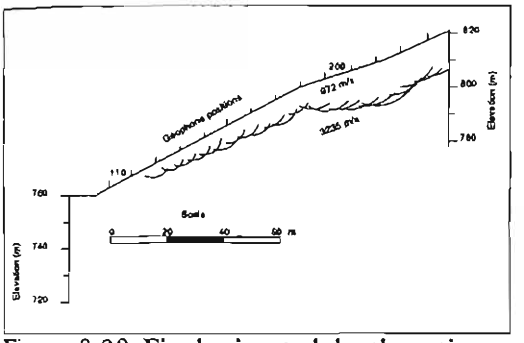

Figure 8.28: Final migrated depth section for profile D-D', Xiakou Landslide, Sichuan, China

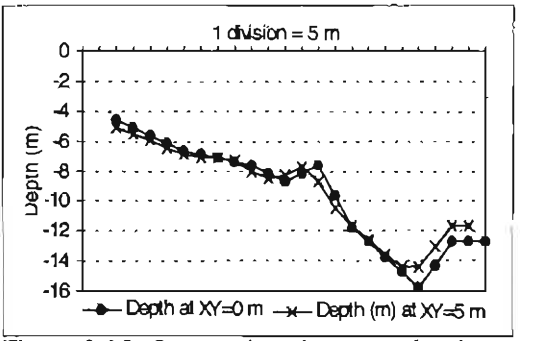

Figure 8.29: Comparison between depths calculated for XY=0 metres (for the t_0 method) and optimum XY=5 m for profile D-D', Xiakou Landslide, Sichuan, China

Prediction of a mudslide using VES: Arniko Highway, Nepal

During the early part of the 1995 monsoon, a few landslides and landslide-prone slopes along the Arniko Highway (which runs between Kathmandu and the Nepal-China border) were studied by seismic refraction and electrical resistivity methods. Resistivity measured by vertical electrical sounding (VES) was useful for locating the depth to water table and studying the types of material and depth to bedrock and/or more stable formations. The wide range of electrical resistivity values for different materials made it possible to use the resistivity methods to predict the possible activation of landslides. In the Dolalghat-Barhabise sector of the highway, the lowest apparent resistivity values were observed at km 74+00. The electrical conductivity value (80 µS/cm) indicated that the groundwater water was fresh. The variation in electrical resistivity of the material in the overburden saturated with this water was due to the variation in grain size: the lower the electrical resistivity, the finer the grain size.

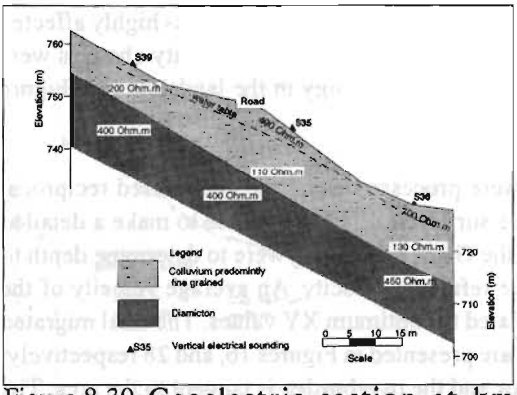

Figure 8.30: Geoelectric section at km 74+00, Arniko Highway, Nepal

Several vertical electric soundings were conducted on the slope to the mountain and valley-side of the highway at km 74+00 (Figure 8.30). The VES measurements showed that the water table was at a depth of 2-3.5m. The electrical resistivity was 110-130 Ω m in the lower part of the profile (valley side), and 200 Ωm and more on the mountain side. The low electrical resistivity on the valley side indicated that the overburden consisted of a predominantly finer matrix, with higher porosity and lower permeability. Since there was the possibility of a further rise in the water table during the monsoon, occurrence of a mudslide was predicted. The road slid a week after completion of the fieldwork.

Study of landslides using 2-D profiling: Arniko Highway, Nepal

In February 1997, a proposal was made to study in detail the subsurface of two landslides at km 85+280 and km 87+700 of the Arniko Highway using electrical resistivity methods. The objectives of the study were not only to investigate the subsurfaces of these landslides but also to work out appropriate methodologies for continuous coverage to enable estimation of types of material in the subsurface. The types of material and the nature of the slides observed at these sites were similar to those observed in other sections of the Barhabise-Kodari section (km 87-114). Thus it was hoped that the findings and methodologies worked out for these landslides could be used in future investigations along the Barhabise-Kodari section as well as other parts of the Arniko Highway.

The landslide surface material was dominated by silt at km 87+700, and by mostly coarse-grained material at km 85+280. There are reports that in 1955 a mudflow from the Sandhi Kholsa (km 87+700) dammed the Bhote Kosi River for a few hours. A shallow mudslide has been reactivated at the Sandhi Kholsa since 1990, and there is a possibility that the Bhote Kosi could again be dammed in the future.

The landslides were studied using 2-D profiling (electrical resistance tomography or ERT) and by conventional vertical electrical sounding (VES). The 2-D profiling was conducted using a pole-pole configuration with a unit electrode spacing of 4m together with some additional measurements at 1, 2, and 3m to get the effect of microsounding. Conventional VES's were conducted using the Schlumberger configuration. The Schlumberger and pole-pole results were compared and the results showed that the pole-pole configuration was less affected by near-surface inhomogeneities and had greater depth penetration. Thus the pole-pole configuration was recommended for future shallow-depth investigations (Pant 1998), especially for mapping shallow landslides. Figures 31-33 show three of the tomogram profiles: one at km 85+280 and two at the Sandhi Kholsa (km 87+700).

The sliding area at km 85+280 seems to be a part of a larger unstable area. Figure 8.31 shows the 2-D profile along the downslope (below road level) at an angle of 32 degrees. The very high electrical resistivity (more than 5000 Ωm) in the model section is indicates a dry, loose, and displaced mass. The maximum thickness of the image (high resistivity zone) is 10-12m. This zone is prone to sliding

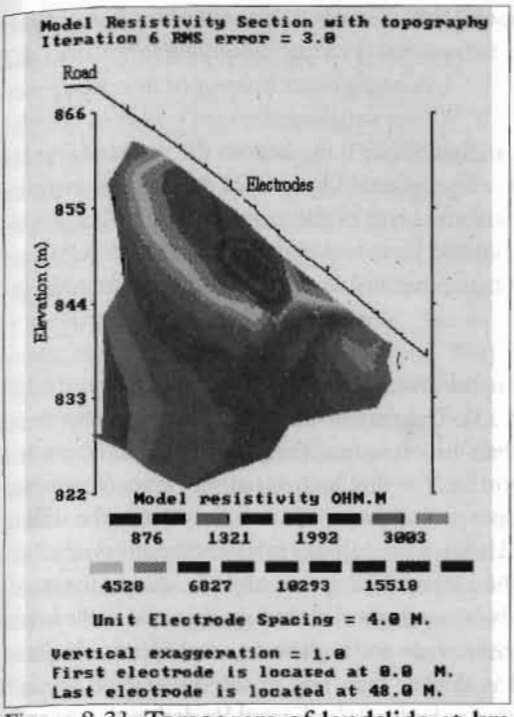

Figure 8.31: Tomogram of landslide at km 85+280, Arniko Highway, Nepal

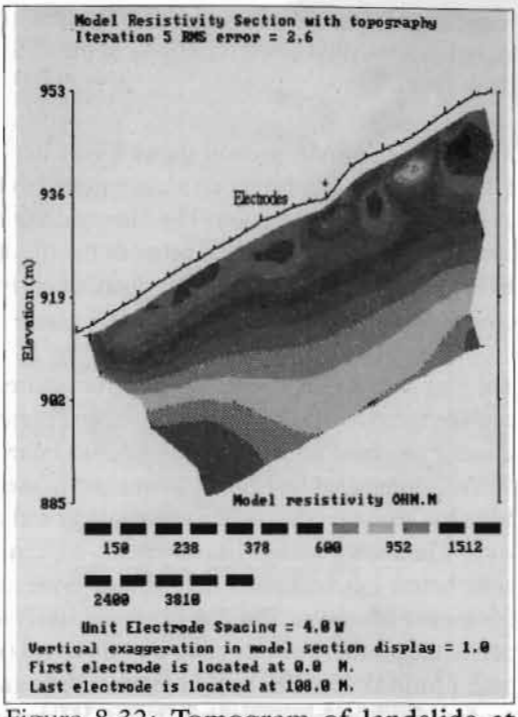

Figure 8.32: Tomogram of landslide at Sandhi Kholsa, Profile One, Arniko Highway, Nepal

during the monsoon. Below this zone the resistivity decreases slowly. From the resistivity distribution pattern at depth it can be inferred that there is no effect from fresh rock. However the low resistivity formation at depth indicated by the tomogram might indicate the presence of fractured and weathered rock.

The 2-D profiles shown for the Sandhi Kholsa (km 87+700) were made at an angle of 45° to each other and in a slope of 20°. The first profile (Figure 8.32) trends north-east to south-west, and the second (Figure 8.33) south-east to north-west; they cross each other at the point denoted by the asterisk. The unit electrode spacings for the first and second profiles were 4 and 5m respectively. Micro-VES measurements using a pole-pole configuration showed the ratio of the resistivity of the slide to the resistivity of the underlying layer to be 3:10. This was interpreted as reflecting differences in rock (lithological) characteristics between the sliding material and the underlying material that serves as the slip surface. The lower part of the slide (silt-domi-

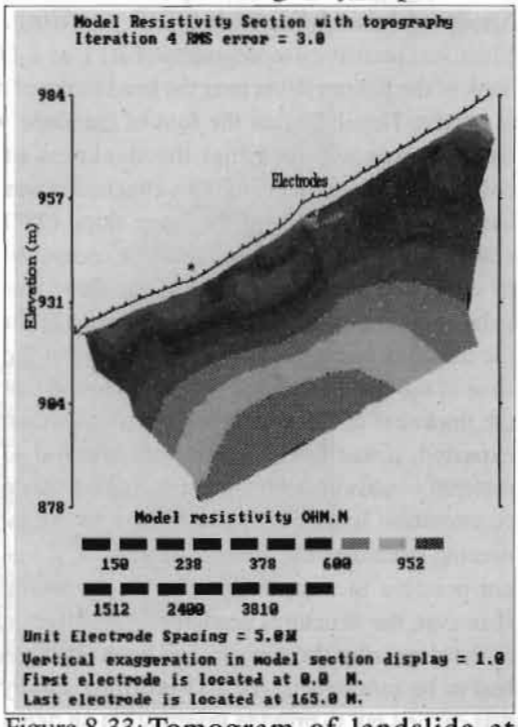

Figure 8.33: Tomogram of landslide at Sandhi Kholsa, Profile Two, Arniko Highway, Nepal

nated material) was developed within the same material type (usually only the case for fine-grained materials); the ratio of the resistivity of the slide to the resistivity of the underlying layer was 1.3:2 (Pant 1998).

The model resistivity section shows a very low-resistivity layer quite near to the surface (Figures 8.32 and 8.33). This layer can be interpreted as the effect of a silt-dominated deposit that is prone to flow during the monsoon. The intermediate-resistivity layer is interpreted as the effect of collapsed rock mass sandwiched between the silt-dominated layer and high-resistivity bedrock (Pant 1998). The pattern of resistivity distribution indicates that the thickness of the overburden increases toward the upslope.

The near-subsurface low-resistivity layer apparent in the lower part of the first profile (Figure 8.32) can't be seen clearly in the second profile (Figure 8.33). This may be because a larger unit electrode spacing was used for the second profile (5 rather than 4m). It seems likely, however, that there is a thin silt-dominated layer at the lower part of the profile. The thin high-resistivity layer (more than 500 Ωm) seen near the surface in the middle and upper part of the profile is mainly due to the sliding layer. The sliding surface lies on the silt-dominated layer. The inability to detect the silt-dominated layer below this high-resistivity sliding layer in the second tomogram might be due to the small thickness of the layer. The sliding layer is likely to be coarser-grained than the material in the lower part of the profile. The other two electric layers (intermediate and high-resistivity) appear similar in both profiles. The overburden at the upper end is thicker than that at the lower end. In both profiles, the high-resistivity substratum is interpreted as bedrock (indicated by dark red colours in the figures).

Study of a landslide using 2-D profiling: Khimti I Hydropower Project, Nepal

Electrical resistivity tomography (ERT), or 2-D profiling, was used to study a slope on the right bank of the Khimti River near the headworks of the Khimti I hydropower project being constructed in eastern Nepal. Before the foot of the slope was excavated during preparations for a desilting basin, it was assumed that the thickness of colluvium was less than 5m. This conclusion was based on the evidence of the steep slope (38°) and the proximity of exposed bedrock composed of schist and gneiss. The base of the slope was to be cut for about 10-15m to prepare the site for the desilting basin. As the loose material at the base of the slope was removed, it was found that the thickness of the colluvium was greater than expected; it was feared that further removal of material would affect the slope stabilisation. Since construction had already started on the engineering structures for the desilting basin, it was not possible to completely relocate the basin. However, the structures needed for stabilisation of the slope after the material had been removed had to be redesigned. An 2-D profiling survey was carried out to provide information on depth to bedrock, type of material in the overburden, and depth to water table in the slope.

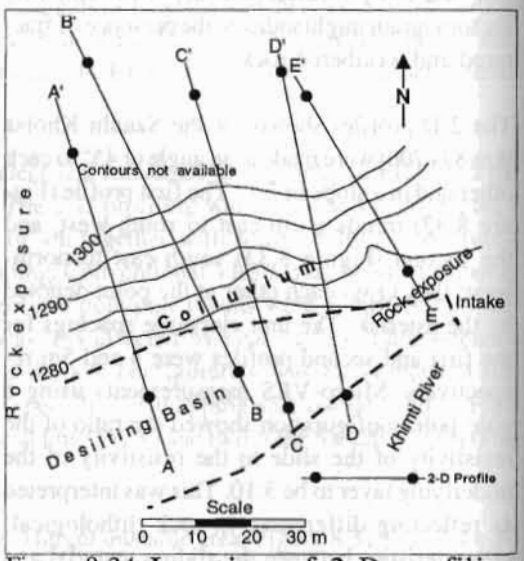

Figure 8.34: Location of 2-D profiling profiles, Khimti I hydropower project, Nepal

Measurements were conducted along five profiles laid along the slope (Figure 8.34). The data were processed to prepare tomograms and 2-D polygon models. One representative profile (C-C') is taken here for discussion. The tomogram is shown in Figure 8.35. It contains an image of very high electrical resistivity (>5000 Ωm) extending from the surface to a depth of about 12-15m. The image below the yellow colour is produced by rock that is below the water table. The expected bedrock is jointed and weathered. Very high electrical resistivity values (probably more than 9000 Ωm) indicate the presence of very loose and dry material within the overburden in the lower and central part of the profile.

The data used to prepare the tomogram were also processed to prepare a polygon model, and these results used to prepare geoelectric sections. The geoelectric section for profile C-C' is shown in Figure 8.36. The very high electrical resistivity layer indicates mainly loose and dry overburden. The VES results indicated the presence of a saturated alluvial deposit in the lower part of the profile. Bedrock is represented by relatively low resistivity. The body in the section with a resis-

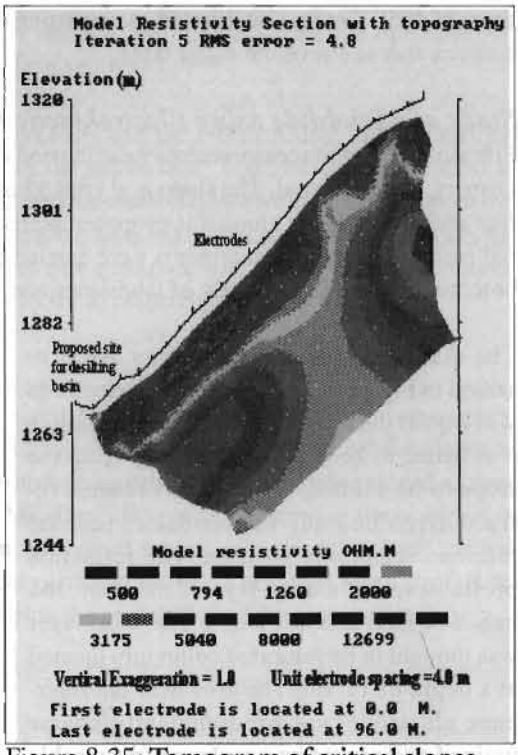

Figure 8.35: Tomogram of critical slopes for profile C-C' near the Khimti I hydropower project, eastern Nepal

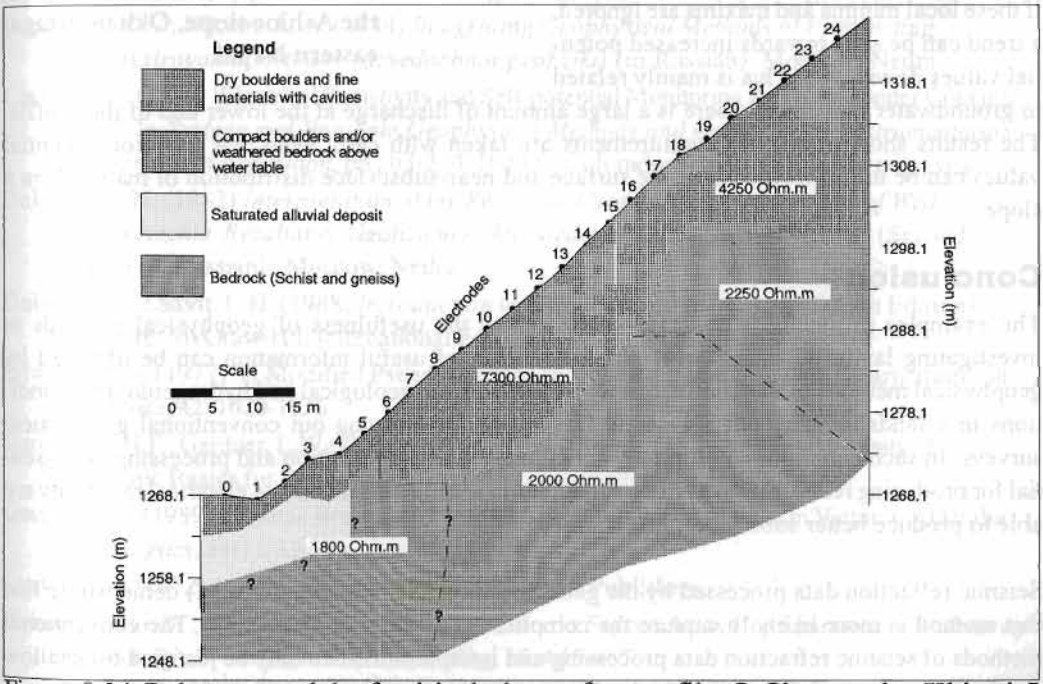

Figure 8.36: Polygon model of critical slopes for profile C-C' near the Khimti I hydropower project, eastern Nepal.

tivity of 4250 Ωm was interpreted as consisting of compact boulders and fine material, and may be bedrock that is above the water table.

Study of a landslide using Electrokinetic (Filtration) potential: Okhaldhunga, Nepal

Filtration potential measurements were carried out on the slope of Ashine village in Okhaldhunga District, eastern Nepal. The slope is at km 157 of the proposed Gaighat-Okhaldhunga Highway. A few additional slopes along this proposed highway were also investigated by the filtration potential method. These measurements were carried out to demonstrate the usefulness of the filtration potential method in the study of landslides and critical slopes.

The Ashine slope measurements are presented in Figure 8.37. The reference electrode was kept at the middle of the profile, although it is better to keep electrodes away from the slope to be studied. A very short seismic refraction profile study was conducted near the reference electrode position. The refraction profile revealed a three-layered medium: 365 m/s, 674 m/s, and 1561 m/s. The third layer was thought to be saturated colluvium located at a depth of 11.5m. The area near the reference electrode was predominantly coarse grained and served as a recharge (permeable zone). The upper and lower parts of the slope had several permeable and impermeable beds indicated in the figure as local lows and highs. If these local minima and maxima are ignored, a trend can be seen towards increased potential values downslope. This is mainly related to groundwater movement; there is a large amount of discharge at the lower end of the profile. The results show that if the measurements are taken with care, even low filtration potential values can be useful for mapping the surface and near-subsurface distribution of materials in a slope.

Figure 8.37: **Filtration potential observed on the Ashine slope, Okhaldhunga, eastern Nepal**

Conclusion

The examples presented in the case studies show the usefulness of geophysical methods in investigating landslide subsurfaces. A large amount of useful information can be obtained by geophysical methods in a cost-effective way. However, the geological and hydrogeological conditions in a landslide may not always be favourable for carrying out conventional geophysical surveys. In such situations, appropriate techniques for data acquisition and processing are essential for producing reliable results. New techniques in seismic refraction and electrical resistivity are able to produce better subsurface information.

Seismic refraction data processed by the generalised reciprocal method (GRM) demonstrate that this method is more likely to capture the complicated geology of a landslide. The conventional methods of seismic refraction data processing and interpretation can only be justified for shallow depths. The velocity information obtained by conventional methods is affected by bedrock topography and near-surface lateral inhomogeneities – situations often met in landslide areas. In con-

trast, the velocity information obtained by GRM is reliable, and the velocities and optimum XY values can be used to generate a migrated subsurface section.

The electrical resistivity tomograms of the landslides show that the 2-D profiling, or ERT, method is capable of producing detailed information about the subsurface. The method can be used to separate sliding masses from intact masses and slip surface materials by virtue of the high resistivity contrasts. However, if there is fine material in the near-subsurface that is prone to mudslide, the resistivity difference between the sliding and intact fine materials will not be very high. Good-quality bedrock is always indicated by very high electrical resistivity values.

Acknowledgements

The author is thankful to Dr. John M. Reynolds for his reading and comments during the preparation of this paper. The author is grateful to the Arniko Highway Project and the owner and developer of the Khimti I Hydropower Project for granting permission to publish the materials enlisted as case studies in this paper. I extend my sincere thanks to Mr. Alexis Wagner for reviewing the materials in the case studies; he has always emphasised the importance of investigating landslides and critical slopes along the highways of Nepal by geophysical methods. Finally, I am thankful to Prof. B.N. Upreti and Prof. Li Tianchi for their suggestions during the preparation of the manuscript.

References

Bogoslovsky, V.A.; Ogilvy, A.A.; Strakhova, N.A. (1977) 'Magnetometric and Electrometric Methods for the Investigation of the Dynamics of the Landslide Processes'. In *Geophysics Prospect,* 25: 280-291

Bogoslovsky, V.A.; Ogilvy, A.A. (1970) 'Natural Potential Anomalies as a Quantitative Index of the Rate of Seepage from Water Reservoirs'. In *Geophysical Prospecting*, 18(2): 261-268

Brodovoe, V. V.; Nikitin, A. A. (1984) *Integrating Geophysical Methods of Prospecting (Complexirovania metodov razvedochnoi geofiziki)* (in Russian). Moscow: Nedra

Corwin, F.R. (1986) 'Electrical Resistivity and Self-potential Monitoring for Groundwater Contamination'. In *Surface and Borehole Geophysical Methods and Groundwater Instrumentation Conference and Exposition,* pp 203-214. Denver, Colorado: Name of Publisher not given

Dakhnov, V.N. (1982) *Interpretation of the Results of Geophysical Investigation of Wells (Interpretachia Rezultatov Geofizicheskikh Isledovanii Razrezov Skvajhin)* (Second edition) (in Russian). Moscow: Nedra

Dobrin, M.B.; Savit, C.H. (1988) *Introduction to Geophysical Prospecting* (Fourth Edition). Singapore: McGraw-Hill International Editions

Edwards, L.S. (1977) 'A Modified Pseudo-Section for Resistivity and Induced Polarization'. In *Geophysics*, 42: 1020-1036

Gardner, G.H.F.; Gardner, L.W.; Gregory, A.R. (1974) 'Formation Velocity and Density- The Diagnostic Basics for Stratigraphic Traps' In *Geophysics*, 39: 770-780

Geissler, P.E. (1989) 'Seismic Reflection Profiling for Groundwater Studies in Victoria, Australia'. In *Geophysics*, 54(1): 31-37

Gurvich, I.I. (1972) *Seismic Prospecting*. Moscow: Mir Publishers

Habberjam, G. M.; Watkins, G. E. (1967) 'The Use of a Square Array Configuration in Resistivity Prospecting'. In *Geophysical Prospecting*, 15: 445-467

Hagedoorn, J.G. (1959) 'The Plus-Minus Method of Interpreting Seismic Refraction Sections'. In *Geophysical Prospecting* , 7(2):158-182

Keller, G. V.; Frischknecht, F. C. (1966) *Electrical Methods in Geophysical Prospecting*. London: Pergamon

Klushin, I.G. (1968) *Integrated Application of Geophysical Methods for Solving Geological Problems (Complexirovannoe primenenia geofizicheskikh metodov dlya reshenia geologicheskikh zadach)* (in Russian). Leningrad: Nedra

Lankston, R.W. (1990). 'High-resolution Refraction Data Acquisition and Interpretation'. In Ward, S.H. (ed) *Geotechnical and Environmental Geophysics. Vol. I: Review and Tutorial*, pp 45-73. Tulsa: Society of Exploration Geophysicists

Lankston, R.W., Lankston, M.M. (1986) 'Obtaining Multilayer Reciprocal Times Through Phantoming'. In *Geophysics*, 51: 45-49

Mauritsch, J.H.; Seiberl, W.; Arndt, R.; Romer, A.; Schneiderbauer, K.; Sendlhofer, G.P. (2000) 'Geophysical Investigations of Large Landslides in the Carnic Region of Southern Austria'. In *Engineering Geology*, 56:373-388

Novitskii, G. P. (1974) *Integrating Geophysical Methods of Investigation (Complexirovannia geofizicheskikh metodov razvedki)* (in Russian). Leningrad: Nedra

Oldenburg, D.W.; Li, Y. (1999) 'Estimating Depth of Investigation in DC Resistivity and IP Surveys'. In *Geophysics*, 64(2):403-416

Palmer, D. (1981) 'An Introduction to Generalized Reciprocal Method of Seismic Refraction Interpretation'. In *Geophysics*, 46:1508-1518

Pant, S.R. (1998) 'Use of Pole-Pole and Schlumberger Electrode Arrangements of Electrical Resistivity Survey of Landslides along Arniko Highway'. In *Bull. Dept. Geology, Tribhuvan Univ.*, 6:31-42

Pant, S.R.; Li, T.; Wagner, A.; Wei, F.; Jiaman, C. (1999). 'High Resolution Seismic Refraction Data Interpretation: An Example from Xiakou Landslide, Sichuwan, China'. In *Jour.Nepal Geol.Soc.*, 19:31-40

Parasnis, D.S. (1997) *Principles of Applied Geophysics*, Fifth Edition, London: Chapman & Hall

Reynolds, J.M. (1997) *An Introduction to Applied and Environmental Geophysics*. England: John Wiley & Sons

Robinson, S. E.; Coruh, C. (1988) *Basic Exploration Geophysics*. USA: John Wiley & Sons

Schiavone, D.; Quarto, R. (1984) 'Self Potential Prospecting in the Study of Water Movements. In *Geoexploration*, 22: 47-58

Semenov, A.S. (1974) *Electrical Methods of Natural Electrical Fields (Elektropazbedka metodom estectvennogo elektricheskogo polya)*, (in Russian). Leningrad: Nedra

Sheriff, R.E.; Geldart, L.P. (1982) *Exploration Seismology (Seismorazvedka), Vol.1* (Translated into Russian). Moscow: Mir

Telford, W.M.; Geldart, L.P.; Sheriff, R.E.; Keys, D.A. (1976) *Applied Geophysics*, 2nd edn. Cambridge: Cambridge University Press

Wenner, F. (1912) 'A Method of Measuring Earth Resistivity'. In *US Bureau of Standards Bulletin*, 12:469-478

Wyllie, M.R.; Gregory, A.R; Gardner, G.H.F. (1958) 'An Experimental Investigation of Factors Affecting Elastic Wave Velocities in Porous Media'. In *Geophysics*, 23(3) 459-493